TO BE SUBMITTED TO APJ
Preprint typeset using LATEX style emulateapj v. 10/09/06

THE FATE OF THE FIRST GALAXIES. III. PROPERTIES OF PRIMORDIAL DWARF GALAXIES AND THEIR IMPACT ON THE INTERGALACTIC MEDIUM

MASSIMO RICOTTI[1], NICKOLAY Y. GNEDIN[2,3,4], AND J. MICHAEL SHULL[5]

(Received .....; Accepted .....)
to be submitted to ApJ

ABSTRACT

In two previous papers, we presented simulations of the first galaxies in a representative volume of the Universe. The simulations are unique because we model feedback-regulated galaxy formation, using time-dependent, spatially-inhomogeneous radiative transfer coupled to hydrodynamics. Here, we study the properties of simulated primordial dwarf galaxies with masses $\lesssim 2 \times 10^8$ M$_\odot$ and investigate their impact on the intergalactic medium. While many primordial galaxies are dark, about 100–500 per comoving Mpc^3 are luminous but relatively faint. They form preferentially in chain structures, and have low surface brightness stellar spheroids extending to 20% of the virial radius. Their interstellar medium has mean density $n_H \approx$ 10–100 cm^{-3}, metallicity $Z \sim 0.01$–0.1 Z$_\odot$ and can sustain a multi-phase structure. With large scatter, the mean efficiency of star formation scales with halo mass, $\langle f_* \rangle \propto M_{\rm dm}^2$, independent of redshift. Because of feedback, halos smaller than a critical mass, $M_{crit}(z)$, are devoid of most of their baryons. More interestingly, we find that dark halos have always a smaller $M_{crit}(z)$ than luminous ones. Metal enrichment of the intergalactic medium is inhomogeneous, with only a 1%–10% volume filling factor of enriched gas with [Z/H]> -3.0 and 10%–50% with [Z/H] > -5.0. At $z \approx 10$, the fraction of stars with metallicity $Z < 10^{-3}$ Z$_\odot$ is 10^{-6} of the total stellar mass. Although detections of high-redshift dwarf galaxies with the *James Webb Space Telescope* will be a challenge, studies of their fossil records in the local Universe are promising because of their large spatial density.

Subject headings: early universe —cosmology: galaxies: dwarf — galaxies: formation — intergalactic medium — methods: numerical

1. INTRODUCTION

In cold dark matter (CDM) cosmologies, the first galaxies in the universe are predicted to have been about 10^6 times smaller than the Milky Way, with characteristic masses comparable to mass estimates for the smaller dwarf spheroidal galaxies (dSph) observed around our Galaxy and Andromeda (Mateo 1998; Belokurov et al. 2007). The gravitational potentials of these 10^{6-8} M$_\odot$ objects are so weak that the warm and hot ionized phases of their interstellar medium (ISM) are weakly bound. As a result, each episode of star formation may produce powerful outflows that could temporarily inhibit further star formation.

For the sake of brevity, we hereafter refer to "dwarf primordial" (dPri) galaxies to indicate galaxies with virial temperature $T_{\rm vir} \lesssim 20,000$ K (or circular velocity $v_c \lesssim 20$ km s^{-1}). In contrast to more massive galaxies, the dark matter (DM) halos of dPri galaxies are too shallow to contain much photoionized gas with temperatures 10,000–20,000 K. During their formation, the gas is heated to temperatures below 10^4 K, where it is unable to cool by atomic hydrogen (Lyα) line emission. The mass of these DM halos is $M_{\rm dm} \lesssim 2 \times 10^8$ M$_\odot$ at their typical redshifts of formation (redshift $z \gtrsim 10$). These galaxies rely primarily on the formation of molecular hydrogen (H_2) to cool and form stars, because metal cooling is negligible as long as the gas has almost primordial composition. This situation changes, after the metallicity of the intergalactic medium (IGM) rises above a critical value, $Z_{\rm crit}$, which could be as large as 1% solar (Santoro & Shull 2006) at halo gas densities $n_H \approx$ 10–100 cm^{-3}. As the first few stars are formed, these requirements no longer hold, since some gas is heated above 10,000 K and is polluted with heavy elements.

The relevance of understanding the formation of the first galaxies is not purely academic. Instead, it is closely connected to many outstanding questions in cosmology, including:
(1) The *Wilkinson Microwave Anisotropy Probe* (WMAP) satellite has detected a polarization signal in the cosmic microwave background radiation (CMB) that indicates that the optical depth to Thomson scattering is $\tau_e \simeq 0.09 \pm 0.03$ (Spergel et al. 2007). This result may require massive star formation at redshift $z > 6$ (Haiman & Bryan 2006; Shull & Venkatesan 2008), along with partial ionization by X-rays from intermediate-mass black holes (BHs) in the first galaxies (Ricotti & Ostriker 2004b; Madau et al. 2004; Venkatesan et al. 2001; Oh 2001).
(2) The eventual formation of seed BHs in dPri galaxies can be important for the assembly of supermassive black holes in the bulges of galaxies and the nature of ultralu-

[1] Department of Astronomy, University of Maryland College Park, MD 20742. E–mail: ricotti@astro.umd.edu
[2] Particle Astrophysics Center, Fermi National Accelerator Laboratory, Batavia, IL 60510. E–Mail: gnedin@fnal.gov
[3] Department of Astronomy and Astrophysics, University of Chicago, Chicago, IL 60637
[4] Kavli Institute for Cosmological Physics, University of Chicago, Chicago, IL 60637
[5] CASA, Department of Astrophysical & Planetary Sciences University of Colorado, 389-UCB, Boulder CO 80309. E–mail: mshull@casa.colorado.edu

minous X-ray (ULX) sources observed in nearby galaxies (e.g., Miller et al. 2003).
(3) Future radio observations of redshifted 21 cm emission from gas at $6 < z < 10$ will probe the ionization and thermal history of the IGM prior to reionization (e.g., Madau et al. 1997), when dPri galaxies could be the dominant population.
(4) The origin of the metals observed in the low-density Lyα forest at redshifts $z \sim 2-5$ is an argument of debate (Simcoe et al. 2004). One view invokes nearly uniform IGM pre-enrichment produced by the first stars at high-redshift (Madau et al. 2001). The other view attributes the origin of the observed metal lines to hot, metal-enriched superbubbles located around Lyman-break galaxies (Adelberger et al. 2003). Given the difficulties associated with both scenarios, it is important to know the amount and volume filling factor of metal-enriched IGM produced by dPri galaxies.
(5) If a substantial population of dPri galaxies existed at redshift $z \simeq 10$, we expect that about 10% of these galaxies may survive without further mergers to the present (Gnedin & Kravtsov 2006). It is a fascinating possibility that some of the dSph galaxies observed in the Local Group could be identified as the few well-preserved fossils of dPri galaxies (Ricotti & Gnedin 2005).
(6) Finally, a new generation of large telescopes will push the frontiers of the observable universe to the ages when this primordial galaxy population is forming. Given the current uncertainties on their importance or even their existence, it is crucial to make reliable models to predict what these telescopes might observe. In particular, infrared observations with the *James Webb Space Telescope* (*JWST*) or the *Giant Segmented Mirror Telescope* (GSMT) should be able to constrain theories for the formation of the first galaxies.

In order to help understand some of the aforementioned cosmological problems it is essential to know whether a cosmologically significant number of dPri galaxies formed and to predict their cosmological impact. Despite recent progress, the answer to this question is controversial, largely because of the uncertain effects of radiative and dynamical feedback from galaxy formation. In two previous papers (Ricotti et al. 2002a,b, hereafter Papers 1 and 2, respectively) we described our cosmological simulations of high-redshift galaxy formation with radiative feedback from star formation. Those papers dealt primarily with implementing radiative transfer in the ionizing continuum and understanding both "positive and negative feedback" on the formation and destruction of H_2. We found significant effects of "radiative feedback" on the first galaxies and processes of reionization, from redshifts $z \approx 30 \rightarrow 10$.

Our current study (Paper 3) focuses on simulation results on the population of dwarf primordial galaxies. This paper is organized as follows. In § 2 we describe the set of cosmological simulations that we analyze in this work. In § 3, we introduce and discuss the feedback processes that may determine the frequency of the dPri galaxies. We analyze the cooling mechanisms and large scale clustering properties (bias) of galaxies to understand which physical processes are involved in the self-regulation of star formation and which is dominant. In § 5 we discuss the processes that eject metals from the galaxies and their importance for the enrichment of the IGM. In § 6 we analyze statistical properties of dPri galaxies such as their mean stellar and baryon fraction. We also study their internal properties: the ISM and the properties of their stellar and dark halos. In § 7 we address the observability of primordial galaxies at high redshift with the *JWST*. We also address the prospects for the identification of their fossil records in the local Universe, noting that this topic has been investigated in greater detail in separate papers (Ricotti & Gnedin 2005; Gnedin & Kravtsov 2006; Bovill et al. 2008). We show that most low-mass galaxies in the Local Group are expected to be either dark or too faint to be detected[6]. Therefore, the so called "missing satellite problem" (Moore et al. 1999) for the Milky-Way and Andromeda is not a fundamental challenge to Cold Dark Matter cosmology. We present a summary of our results in § 8.

2. SIMULATION DATA

In this work, we study in greater detail the statistical properties of dPri galaxies in a set of simulations from Paper 2 that include strong and weak radiative feedback (runs S1, S2, S3 and S4 in Table 1). In addition we analyze three simulations from Ricotti & Ostriker (2004b); Ricotti et al. (2005) (hereafter, RO04 and ROG05) that include pre-ionization by X-rays (run S5) and early ionization by Pop III stars with weak and strong SN feedback (run S6 and S7 respectively). In all the simulations we use a fast method to solve three-dimensional radiative transfer of H I , He I and He II ionizing radiation and follow the non-equilibrium chemistry of neutral and molecular hydrogen and helium. We simulate a cosmologically representative volume of the universe with initial conditions drawn from the concordance flat, cold dark matter cosmology with cosmological constant (ΛCDM). We stopped the simulations at redshift $z \sim 8-10$ because of their small volume. We included a phenomenological description of star formation and, in some simulations, the effects of SN feedback.

Our simulations are tailored to study stellar feedback on the baryon content and star formation in galaxies with masses $M_{\rm dm} \lesssim 10^9$ M$_\odot$ (i.e., virial temperatures $T_{\rm vir} \lesssim 4 \times 10^4$ K). In our higher resolution simulation we are able to examine the properties of single objects in detail, since they are resolved with 10,000–50,000 DM particles and $\sim 10,000$ stellar particles. We also analyze the importance of dPri galaxies for metal enrichment of the high-z IGM. We attempt to understand in more detail the mechanisms that trigger and suppress star formation, and the internal properties of the galaxies that can help us to distinguish these objects from more massive galaxies that did form at later times by Lyα cooling. Ricotti & Gnedin (2005) further evolved the high-resolution simulation, including the effects of reionization, and compared the properties of the simulated galaxies at redshift $z \sim 8$ with dSph galaxies observed in the Local Group. They found that the proper-

[6] In the last two years, data mining of the Sloan Digital Sky Survey has revealed the existence of an ultra-faint population of dwarf spheroidal galaxies that has the same properties as predicted by our simulations (Ricotti et al. 2002b; Ricotti & Gnedin 2005; Bovill et al. 2008). The galactocentric distribution around the Milky-Way is in agreement with predictions for the fossils of the first galaxies (Gnedin & Kravtsov 2006; Bovill & Ricotti 2008).

TABLE 1
List of simulations with radiative transfer.

Short Name	RUN	N_{box}	L_{box} h^{-1} Mpc	Mass Res. h^{-1} $M_\odot$	Res. h^{-1} pc	g_ν	$\epsilon_{UV}\langle f_{esc}\rangle$	ϵ_*	Comment
S1	256L1p3[d]	256	1.0	4.93×10^3	156	III[a]	2.5×10^{-6}	0.1	high resolution run
S2	128L1p2-2[d]	128	1.0	3.94×10^4	488	II[b]	1.1×10^{-7}	0.05	positive feedback
S3	128L1f1	128	1.0	3.94×10^4	781	II	1.6×10^{-5}	0.2	negative feedback
S4	128L1noRAD	128	1.0	3.94×10^4	781	-	0	0.2	without feedback
S5	128L1XR[d]	128	1.0	3.94×10^4	488	II	1.6×10^{-5}	0.2	"X-ray preionization"
S6	128L2BH[d]	128	2.0	3.15×10^5	976	III	1.6×10^{-5}	0.2	"PopIII → black holes"
S7	128L2PI[d]	128	2.0	3.15×10^5	976	III	1.6×10^{-5}	0.2	"PopIII → PI SNe"

Note. — Parameter description. *Numerical parameters:* N_{box}^3 is the number of grid cells, L_{box} is the box size in comoving h^{-1} Mpc and the resolution is in comoving h^{-1} pc. *Physical parameters:* g_ν is the normalized SED (II = Population II and III = Population III), ϵ_* is the star formation efficiency, ϵ_{UV} is the ratio of energy density of the ionizing radiation field to the gas rest-mass energy density converted into stars (depends on the IMF), and $\langle f_{esc}\rangle$ is the escape fraction of ionizing photons from the resolution element. Models 1-4 are from Paper 1 and are consistent with reionization at $z_{rei} = 6$. Model 5 is from ROG05 and describe a scenario with early pre-ionization by X-rays. Models 6-7 are from RO04 and describe an early Population III reionization consistent with WMAP-1.
[a] g_ν is modified assuming $\langle f_{esc}\rangle = 0.1$, $a_0 = N_{HeI}/N_{HI} = 0.01$ and $a_1 = N_{HeII}/N_{HI} = 10$ where N_i is the column density of the species/ion i (see Paper 1).[b] g_ν is modified assuming $\langle f_{esc}\rangle = 0.01$, $a_0 = 0.1$, $a_1 = 10$.[d] Secondary ionizations included.

ties of most dSph galaxies are consistent with being the fossils of this first population of galaxies.

3. FEEDBACK-REGULATED GALAXY FORMATION

Since the earliest works (e.g., Couchman & Rees 1986) it has been realized that in CDM cosmologies, the first subgalactic structures form as a consequence of the collapse of rare dark matter density perturbations with masses of $10^5 - 10^6$ $M_\odot$ at redshifts $z \sim 30 - 40$. The initial gas cooling must be provided by collisionally excited H_2 rotational and vibrational transitions. Tegmark et al. (1997) estimated that a minimum H_2 abundance of $x_{H_2} \approx 10^{-4}$ is required to trigger star formation in a dark halo in less than a Hubble time. In a dust-free gas, H_2 formation is catalyzed by the H^- ion, that forms as a consequence of the shocks that partially ionize and heat the gas during the virialization process. At a given redshift, the mass of the smaller halo that can form stars is determined by its virial temperature and therefore by its mass. This analytical result has been confirmed by hydrodynamical cosmological simulations. Abel et al. (2002) carried out such numerical simulations for a selected 10^6 $M_\odot$ halo, using adaptive mesh refinement, that resolves the collapse over a large range of scales. They find that, in this selected halo, only one star with mass between 10–100 $M_\odot$ will probably form. Bromm et al. (1999) have also found similar results using a variety of initial conditions for the protogalaxies. These numerical results confirm longstanding theoretical arguments that the first stars should be massive: their characteristic mass reflects the larger Jeans mass in the inefficiently cooling metal-free gas. However, the cooling by trace-metal fine-structure lines depends on the gas density (Santoro & Shull 2006) and coupling with the cosmic microwave background. Thus, the Jeans Mass and "critical metallicity" are sensitive to the gas density in the halos.

Because of space constraints, we will not discuss the many papers on the importance of Population III stars and the first galaxies for reionization (see Venkatesan, Tumlinson, & Shull 2003 and references therein). The typical mass and initial mass function of the first stars is still not well constrained, because of the uncertain role of radiative feedback during the final phases of the protostellar collapse. Even more uncertain is the impact of the first stars compared to Population II. This depends on how many Population III stars can form and the duration of time until they are outnumbered by normal Population II stars (Ricotti & Ostriker 2004a).

3.1. *Negative feedback*

After the first few stars formed, the Universe becomes difficult to model. The H_2 photodissociating radiation in the Lyman-Werner bands ($11.3 - 13.6$ eV) emitted by the stars themselves can destroy H_2 and inhibit gas cooling. In addition, the H I ionizing radiation (ultraviolet and X-ray photons) emitted by hot stars, black holes, and SN remnants may become important or dominant in producing the H^- that catalyzes H_2 formation (e.g., Haiman et al. 1996; Ferrara 1998; Ricotti et al. 2001; Ahn & Shapiro 2007; Whalen & Norman 2008). The formation of H_2 from collisionally ionized gas during virialization is still important, but it might become a subdominant effect, especially if galaxies are clustered, as observed today. The first semianalytic (Haiman et al. 2000) and numerical (Machacek et al. 2001) studies on the radiative feedback from the first galaxies included the effects of an H_2 dissociating background produced by hot stars. In these models, the formation of dPri galaxies is strongly suppressed by the H_2 photodissociating radiation. As a result, efficient and widespread star formation in the universe is delayed until the collapse of more massive DM halos ($M_{\rm dm} \gtrsim 10^9$ $M_\odot$) at later times ($z \gtrsim 15$) formed by Lyα cooling (Oh & Haiman 2002). Yoshida et al. (2003) and Tassis et al. (2003) have also performed simulations on the collapse of pre-galactic clouds, finding that for radiation in the H_2 Lyman-Werner bands with flux $J > 10^{-23}$ ergs s^{-1} cm^{-2} Hz^{-1} sr^{-1}, H_2 molecules are rapidly dissociated, rendering the gas cooling inefficient. They both find that dwarf-sized dark matter halos assembled prior to reionization are

able to form stars and show large variations in their gas content because of stellar feedback and photoionization effects.

3.2. *Positive feedback regions*

Local feedback effects were not included in the aforementioned simulations. Ricotti et al. (2001) demonstrated the importance of "positive feedback", finding that shells of H_2 can be created continuously both in precursors around the Strömgren spheres produced by ionizing sources and, for a bursting mode of star formation, inside recombining H II regions. Recent studies have confirmed the existence and importance of positive feedback regions (Johnson & Bromm 2007; Ahn & Shapiro 2007; Whalen & Norman 2008) in greater detail.

This local positive feedback could be important, but it is difficult to incorporate into cosmological simulations because the implementation of spatially inhomogeneous, time-dependent radiative transfer is computationally expensive and challenging. In Paper 1 we used a fast method to solve radiative transfer coupled to hydrodynamics in cosmological simulations of a representative volume of the Universe. In Paper 2 we explored the importance of different feedback processes in producing what appears as a self-regulated star formation mode on cosmological scales.

The main parameters that regulate the global star formation rate at high-redshift are $\langle f_{esc} \rangle$, defined as the fraction of ionizing radiation that escapes from the simulation resolution element, and the initial mass function (IMF) of the stars. The intensity of the H_2 dissociating background and the assumed efficiency of star formation have, surprisingly, only a minor effect on the self-regulation of star formation. Adopting a Salpeter IMF and $\langle f_{esc} \rangle \lesssim 1\%$, we showed that dPri galaxies may account for most of the stellar mass at redshift $z \sim 9$. If the IMF is top-heavy, or if $\langle f_{esc} \rangle \sim 1$, the global star formation is reduced but not fully suppressed. Internal sources of ionizing photons such as massive stars or quasars produce galactic winds in dPri galaxies that regulate their star formation rates by reducing the gas supply. As a consequence, their star formation history is characterized by several short starburst episodes. The total fraction of stars produced in primordial galaxies depends on the intensity of these bursts of star formation. From the simulations, it appears that dPri galaxies cannot reionize the low-density regions of the IGM because the Strömgren spheres never reach the overlap phase. However, they can produce and eject a substantial mass in heavy elements.

Machacek et al. (2003) studied the effect of a moderate X-ray background on the formation of the first galaxies, finding that they have a minor effect on the global star formation rate. They concluded that the feedback does not completely suppress star formation in low-mass galaxies, in agreement with Paper 2. However, in disagreement with this study, they find that depending on the intensity of the dissociating background, star formation is delayed and less efficient in smaller mass halos. The reason for this disagreement may be their neglect of local feedback such as photoevaporation of the ISM from stellar winds. Susa & Umemura (2004) performed simulations of the effect of reionization on star formation in low-mass galaxies, finding that star formation in halos that collapse prior to reionization is completely suppressed after reionization if the halo is small.

4. LOCAL AND GLOBAL FEEDBACK

In hierarchical models, galaxies form preferentially in groups and filaments. The feedback processes that regulate the cooling of the gas, and therefore star formation in dPri galaxies can be grouped in two categories, with processes labeled as internal (I1, I2, I3) and external (E1, E2, E3, E4):

Internal feedback produced by star formation inside each galaxy: (I1) photoionization by massive stars and mini-quasars is sufficient to evaporate most of the ISM and temporary halt star formation; (I2) galactic winds produced by SN explosions may become important after about 10 Myr; (I3) heavy element self-enrichment affects the ISM properties and possibly the stellar IMF.

External feedback can operate on local scales or on cosmological scales: (E1) the reheating of the IGM produced by ionizing photons (UV and X-rays) increases the Jeans mass of the IGM preventing gas collapse inside the smaller mass halos; this is a negative feedback on cosmological scales; (E2) the radiation backgrounds operate on cosmological scales: the background in the H_2 Lyman-Werner bands (FUV radiation) is a "negative feedback" as it dissociates molecular hydrogen while the X-ray background, increasing the fractional ionization of the gas, may promote H_2 formation and can be a "positive feedback"; (E3) feedback from UV ionizing radiation is a local feedback as it operates on galactic scales. Ionizing radiation produce what we call "positive feedback regions" (Ricotti et al. 2001). These are regions of enhanced H_2 formation located just ahead of ionization fronts and inside recombining H II regions; (E4) contamination of the IGM with heavy elements ejected from neighboring galaxies can promote gas cooling and galaxy formation and should be considered as a "positive feedback".

Although these processes play a role in the regulation of stars and galaxies formation, it is generally possible to identify a dominant feedback process in each simulation. The dominant feedback is determined by the value of the free parameters of the simulation such as $\langle f_{esc} \rangle$, the IMF, and the ionizing spectrum of the sources. In Paper 2 we found that when the efficiency of emission of ionizing radiation per baryon converted into stars is large, for a top-heavy IMF or Salpeter IMF and $\langle f_{esc} \rangle \sim 1$, processes (I1) and (E3) are the dominant feedback mechanisms producing short episodes of bursting star formation in low-mass galaxies. If instead we assume a Salpeter IMF and $\langle f_{esc} \rangle \ll 1$, process (E2) dominates and the dissociating radiation background suppresses the formation of the smaller mass galaxies. Venkatesan et al. (2001) and Ricotti et al. (2005) found that, if the first galaxies host accreting black holes, the IGM is heated to about 10,000 K at redshifts $z \sim 20 - 25$. In this case, process (E1) is effective in reducing star formation in low-mass galaxies (see Fig. 2 in ROG05). Finally, with a top-heavy IMF and mechanical feedback from normal SN or pair-instability SN explosions, process (I2) is important in suppressing star formation also in galaxies more massive than 10^8 $M_\odot$. Metal enrichment (processes [I2] and [E4]) is important in all simulations (see § 4.1).

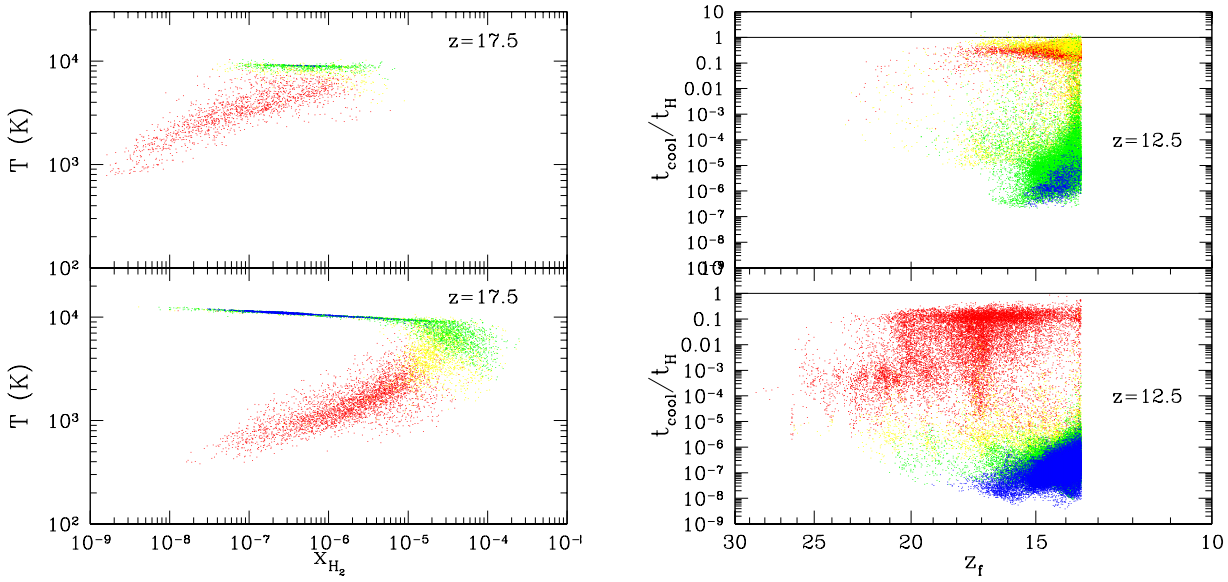

FIG. 1.— (*Left*). Mean molecular hydrogen abundance, x_{H_2}, at $z = 17.5$ as a function of the mean temperature of the sink "stellar particles" in the simulation S2 (top panel) and S1 (bottom panel). (*Right*). Cooling time compared to the Hubble time as a function of the redshift of formation of sink "stellar particles". The top panel is the simulation S2 at $z = 12.5$ and the bottom panel the simulation S1 at $z = 12.5$. In all panels the colors show the metallicity of the star particle: $Z/Z_\odot < 5 \times 10^{-4}$ (red); $5 \times 10^{-4} < Z/Z_\odot < 5 \times 10^{-3}$ (yellow); $5 \times 10^{-3} < Z/Z_\odot < 5 \times 10^{-2}$ (green); and $Z/Z_\odot > 5 \times 10^{-2}$ (blue).

4.1. *Cooling processes*

In this section, we focus on the role of different cooling processes that ultimately lead to the gravitational collapse of the first stars. We show that, after the H_2 in the ISM and IGM is destroyed by the dissociating radiation emitted by the first stars, star formation in a subset of low-mass halos is not suppressed. This is a consequence of the positive feedback from the proximity to already formed galaxies or groups, whose ionizing radiation produces H^- and H_2 (Ricotti et al. 2001). Only a small fraction of the first stars form directly from the collapse of low temperature, zero-metallicity clouds, through cooling by H_2 ro-vibrational transitions. The collapse of most gas clouds is triggered by metal cooling and by Lyα cooling in the photo-heated and metal polluted gas produced by the first stars. Zero metallicity stars are efficient catalysts for further episodes of star formation, not only inside their host halo but also in nearby halos. This has important implications for the clustering and bias properties of the first galaxies, which form preferentially chain-like structures, analogous to young star clusters at low redshift.

Metal enrichment from multiple episodes of star formation within a galaxy (process I2) or metal contamination from neighboring galaxies (process E4) are important in all simulations. H_2 cooling is responsible for the collapse of the first proto-star clusters but subsequently, as the first stars form in a galaxy, their heating and metal pollution provide the dominant cooling mechanisms (Lyα and metal cooling) and they are seeds for further star formation. In Figure 1, we show the temperature versus H_2 abundance of the sink "stellar particles" in two simulations. The figure on the right shows the cooling time, compared to the Hubble time, as a function of the redshift of formation of stellar particles. The top and bottom panels show simulations S2 and S1, respectively. In both panels the colors show the metallicity of the star particle (see caption). Note that in our simulations the star particles lose track of their initial properties when the star formation is continuous, and the metallicity and H_2 abundance of the star particle is the mean mass, weighted over time. When star formation in a cell is stopped by feedback, the star particle is released with its properties. A new particle will be created in the same cell if it experiences a new burst of star formation.

The H_2 abundance in the collapsing "stellar particles" is about $x_{H_2} \sim 10^{-5} - 10^{-6}$, lower than the value $x_{H_2} \sim 10^{-4}$ derived by Tegmark et al. (1997). However, the overdensity in the core of a newly virialized dark halo (i.e., with gas temperature equal to the virial temperature) is about 100 times larger than the mean overdensity $n_{\rm vir}$ adopted in their work. This ensures that, as shown in Figure 1 (right), the cooling time is shorter than the Hubble time at any given redshift. The reaction $H^- + H \rightarrow H_2 + e^-$ that dominates the formation of H_2 absorbs kinetic energy from the gas, producing a net cooling rate that is also important at low temperatures.

In summary, the relative importance of cooling and feedback processes depends on the assumed IMF and $\langle f_{esc} \rangle$. Generally, H_2 cooling is important for the formation of the first few stars in each protogalaxy. After the first episode of star formation, if most gas has not been blown out, Lyα and metal lines become the dominant coolants. The strong clustering of the first dark halos also promotes positive feedback trough metal contamination and photoionization (that promotes H_2 formation) of neighbor galaxies and satellites.

4.2. *Clustering of Primordial Galaxies*

Most galaxies in the Local Volume are approximately located in a sheet or filament also known as the "Supergalactic" plane. Presently, within 5 Mpc from our Galaxy, only about $2 - 3$ faint dwarf galaxies have been discovered that are not associated with any luminous galaxy: Tucana (Lavery & Mighell 1992), Cetus (Whiting et al. 1999), and perhaps the recently discovered Apples1 (Pasquali et al. 2005). The paucity of

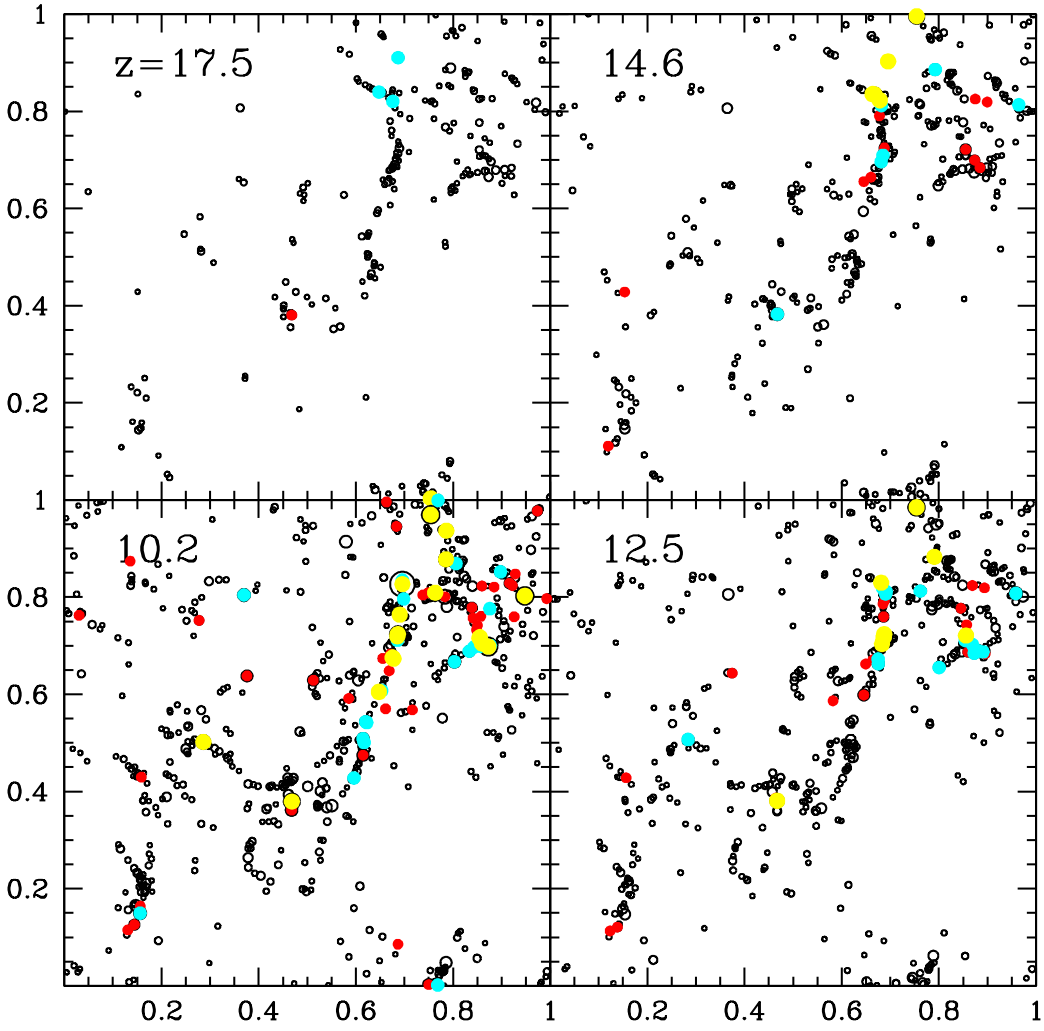

FIG. 2.— Clustering properties of first luminous galaxies. We show positions of dark halos with $M_{dm} > 10^6$ $M_\odot$ in the simulation S1 projected on the $x-y$ plane in a slice with $\Delta z = 0.2\,h^{-1}$ Mpc at $z = 17.5$, 14.6, 12.5, and 10.2 (clockwise from top-left panel). Black circles show halo virial radii, and colored symbols mark halos hosting a luminous galaxy with $L_V > 5 \times 10^5$ $L_\odot$ (yellow), $5 \times 10^4 < L_V < 5 \times 10^5$ $L_\odot$ (cyan) and $L_V < 5 \times 10^4$ $L_\odot$ (red). We assume $M_*/L_V = 1/50$ (solar), appropriate for a young stellar population. Most luminous galaxies seem to form in groups or filaments, with few in isolation in the lower density IGM.

dwarf galaxies out of the Supergalactic plane is a test for models of the formation of dPri galaxies. Unfortunately, the volume of our simulations is too small to allow us to study the spatial distribution of low-mass galaxies at $z = 0$. In order to answer this important question, Bovill & Ricotti (2008) developed a new method to follow the halo evolution of the first galaxies from the redshift of formation to $z = 0$. Already at redshift $z \sim 10$, low-mass galaxies are highly biased, reflecting the importance of local feedback processes in our simulations. Few low-mass galaxies are observed in isolation, and typically these are the faintest of the population.

We find that luminous galaxies form preferentially near previously formed galaxies and are highly biased. This reflects the importance of local positive feedback (i.e., the H_2 precursor in front of H II regions and metal enrichment) in promoting star formation. Figure 2 shows the projected positions of dark halos of mass $M_{\rm dm} > 10^6$ $M_\odot$ in a slice of the run S1 at four different redshifts. The sizes of the black circles are proportional to the virial radii of the dark halos, and the filled circles mark halos hosting luminous galaxies, color coded according to their luminosity: red being the faintest and yellow the brightest galaxies. We have assumed $M_*/L_V = 1/50$ (solar units), appropriate for starbursts at $t \sim 100$ Myr. It appears that luminous galaxies are more clustered than dark halos of the same mass, and line up along the dark matter filaments. Inspecting the four panels in Figure 2, it may appear that a wave of star formation propagates along the dark filaments triggered by the formation of a first galaxy. This is somewhat analogous to what is observed for star clusters in the ISM of galaxies. Although, Figure 2 does not convincely demonstrate the existence of a propagating wave of star formation, the importance of local positive feedback can be demonstrated rigorously. Figure 3 illustrates that the presence of a star bursting

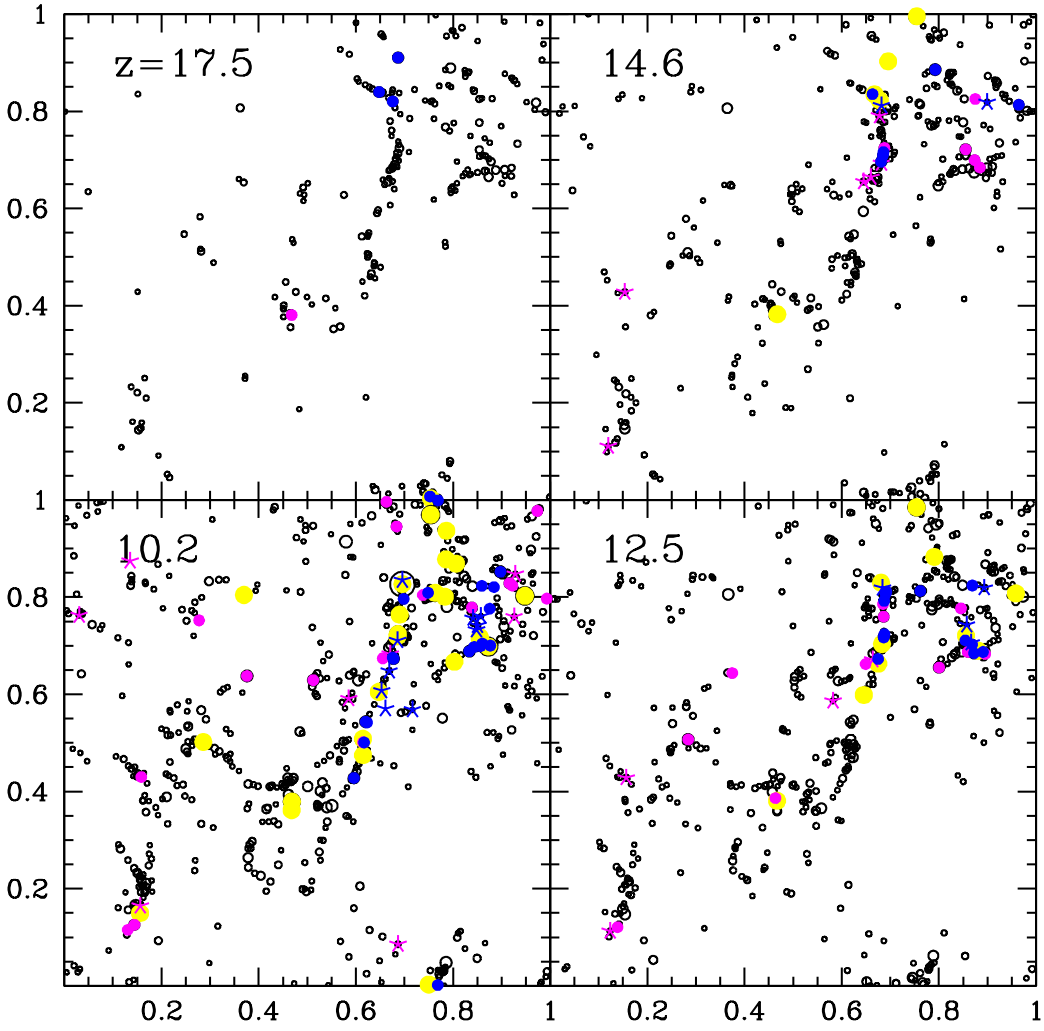

FIG. 3.— Same as in Figure 2 but showing the efficiency of star formation efficiency $f_* = M_*/M_{bar}^{max}$, where $M_{bar}^{max} = M_{dm}\Omega_b/\Omega_m$, rather than the luminosity of dwarf galaxies. Black circles show dark halos with mass $> 10^6$ M$_\odot$ and yellow dots show luminous halos with mass $> 10^7$ M$_\odot$. The blue and magenta symbols show luminous halos with mass $< 10^7$ M$_\odot$ with $f_* > 10^{-3}$ and $f_* < 10^{-3}$, respectively. In addition, luminous halos with a mass $< 3 \times 10^6$ M$_\odot$ are shown as a star rather than a circle. The plots illustrate the importance of local positive feedback in halos with $M < 10^7$ M$_\odot$: halos with identical masses can be either dark or luminous, but are likely luminous if they are nearby another luminous halos.

galaxy enhances the probability and efficiency of star formation, f_*, in nearby low-mass halos. Figure 3 is analogous to Figure 2 but the blue and magenta symbols show luminous halos with mass $< 10^7$ M$_\odot$ with $f_* > 10^{-3}$ and $f_* < 10^{-3}$, respectively. Here, $f_* = M_*/M_{bar}^{max}$, where $M_{bar}^{max} = M_{dm}\Omega_b/\Omega_m$. The yellow circles show luminous galaxies with mass $> 10^7$ M$_\odot$ and the black circles show all dark halos with $M_{dm} > 10^6$ M$_\odot$ as in Figure 2. The reason for dividing luminous galaxies in two groups according to their mass will be evident in § 6. We will show that galaxies of the same mass but with $M_{dm} < 10^7$ M$_\odot$ can be either dark or luminous. Instead more massive halos have a luminosity that is roughly increasing with the halo mass (see Figure 6). Galaxies with mass $< 10^7$ M$_\odot$ are more likely to be luminous and have a high efficiency of star formation (blue circles) if they are nearby other luminous galaxies (e.g., yellow circles) than if they are isolated (e.g., magenta circles). Even galaxies more massive than 10^7 M$_\odot$ are more likely to remain dark (i.e., large black circles) if they evolve in isolation.

5. METAL ENRICHMENT OF THE IGM

Metallicities of about $Z \sim 10^{-3}$ Z$_\odot$ are measured from observation of absorption lines in the Lyα forest at $z \sim 2-5$ (e.g., Songaila 2001; Schaye et al. 2003; Pettini et al. 2003; Simcoe et al. 2004). This mean metallicity, typically inferred from abundances of C IV and Si IV, shows little evolution from $z = 5$ to $z = 2$. However, it is not well understood if a possible redshift-dependent ionization correction may conspire in hiding a real metallicity evolution. The homogeneity of the metal distribution in the IGM is also unknown. This is an important measure, because it can be used to determine the properties of the galaxies responsible for the observed

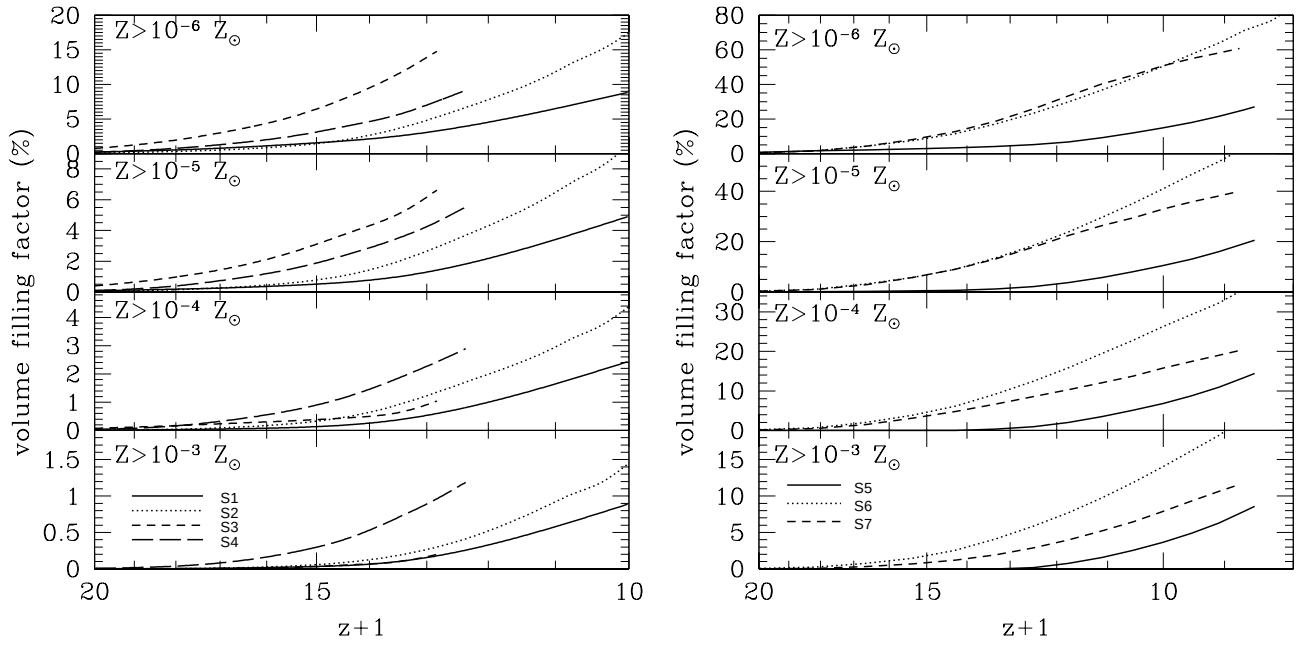

FIG. 4.— Volume filling factor of metal-enriched gas as a function of redshift for the simulations in Table 1. Each panel, from top to bottom, shows the fraction of IGM volume with metallicity $\log(Z/Z_\odot) > -6, -5, -4$ and -3. (Left). These simulations are consistent with models of stellar reionization at $z \sim 6$. In these simulations metals are ejected due to photoevaporation from internal ionizing sources and tidal effects (run S1, S2 and S3) or, as in run S4, by tidal interactions only (long-dashed curves). Simulation S1 (solid curves) is our high-resolution run, S2 and S3 are lower-resolution runs with weak and strong radiative feedback, respectively. Mechanical energy input from SN explosions is not included. (Right) These simulations have typically earlier epoch of reionization, consistent with WMAP-1 and WMAP-3. Here, metals are ejected only due to tidal effects, as in run S6 (dotted curves), by photoevaporation due to X-ray heating, as in run S5 (dashed curves), or by strong SN feedback, as in run S7 (solid curves).

metal enrichment. If underdense regions of IGM contain some metals, then star formation in high-redshift galaxies, of the type studied in this work, may have pre-enriched it (e.g., Madau et al. 2001). If, instead, the metals detected along a line of sight are associated with nearby bright galaxies at $z \sim 2-5$, the metal distribution is probably inhomogeneous. In this second case, observations are not probing a minimum floor of metal enrichment produced by the first galaxies. The current observational sensitivity to metallicity in high-redshift absorbers is $\sim 10^{-3.5} Z_\odot$ (Songaila 2001; Simcoe et al. 2004).

In this section, we analyze the contribution to the IGM metallicity by low-mass galaxies at $z > 8$. We show that the metals produced by the first galaxies can fill the space between bright galaxies uniformly only if we make extreme assumptions on the strength of SN feedback (i.e., in run S6 and S7) and only to very low metallicities floors ($Z/Z_\odot \lesssim 10^{-5}$). For less extreme cases, the volume filling factor is typically $< 10\%$ even at small metallicity floors. Thus, the first galaxies may not able to pollute with metals all the IGM volume, living some large underdense regions of 0.5 comoving Mpc in size (at $z \sim 10$), with primordial composition.

The volume filling factor of the IGM enriched to the typical metallicities observed in the Lyα forest is less than 1% in most runs. It is therefore unlikely that the metal absorption systems associated with the Lyα forest were produced by the very first low-mass galaxies.

In our simulations three different processes can be important in polluting the IGM with metals: (i) metals ejected by galaxy harassment, as proposed by Gnedin (1998); (ii) by galactic winds produced by photoionization in low-mass galaxies (Paper 2); and (iii) by SN explosions (e.g., Ferrara et al. 2000; Madau et al. 2001; Fujita et al. 2004). Using a set of simulations, we can analyze separately the contribution from each process. Before showing the results, we should mention a few caveats. The metal ejection from SN explosions is model dependent, since it is not possible to resolve the multi-phase structure of the ISM and SN shock fronts. We model SN feedback as in Gnedin (1998): energy and metals injection from SNe is local (within the resolution element). We assume perfect mixing of the metals within each cell (i.e., the sub-grid multi-phase medium has homogeneous metallicity). The energy injection from SNe contributes to the heating of the sub-grid multi-phase medium and to increase its velocity dispersion. These terms are calculated using analytical solutions of shocks propagating in a medium with temperature, pressure and density equal to the mean values for the cell. The pressure of the gas includes two terms, for thermal and turbulent pressure. Hence, of the three processes that eject metals into the IGM, only (i) and (ii) are independent of "sub-grid" physics. Finally, the total mass of metals produced and the volume filling factor of gas with metallicity larger than a floor, $Z = Z_0$, is directly proportional to the assumed yields of the stellar population.

In Figure 4 we show the volume filling factor of metal-enriched gas as a function of redshift for a set of simulations listed in Table 1. Each panel, from top to the bottom, shows the volume filling factor of the IGM, $f_V(Z > Z_0)$, that is enriched to metallicities larger than a "floor", Z_0, taken to be 5×10^{-6}, 5×10^{-5}, 5×10^{-4}, and 5×10^{-3} $Z_\odot$. In all our simulations, about 10% of all metals produced end up in the IGM, and the rest resides in galaxies and stars. The metallicity is larger than the mean in overdense regions and lower than the mean

in underdense regions. We should be cautious in comparing the results of the high-resolution simulation with the lower resolution ones, as the metal filling factor may be affected by the numerical resolution. In addition, because of the small box size of the simulations, these metal filling factors become increasingly inaccurate at low redshifts due to the missing clustering on large scales. But galaxy clustering that we miss in will only make the filling factors smaller. Hence the values we calculate should be treated as upper limits.

In the left panels, we show a set of simulations from Paper 2, consistent with models of stellar reionization at $z \sim 6$. In all these simulations, we neglect the mechanical feedback from SN explosions; therefore the metal ejection from the galaxies is produced by tidal stripping of gas or photoevaporation from internal sources, or both. The long-dashed lines refer to run S4 without radiative feedback. All the other lines show runs that include radiative feedback; run S2 with $\langle f_{esc} \rangle = 1\%$ (weak radiative feedback - dotted lines) run S3 with $\langle f_{esc} \rangle = 100\%$ (strong radiative feedback - short-dashed lines), and high-resolution run S1 with $\langle f_{esc} \rangle = 10\%$ (solid line).

In the right panels, we show a set of simulations from RO04 and ROG05, consistent with early IGM reionization suggested by WMAP-1 (optical depth to Thompson scattering $\tau_e \approx 0.17 \pm 0.04$). However, WMAP-3 data (Spergel et al. 2007) imply a lower optical depth, $\tau_e = 0.09 \pm 0.03$, which may be explainable without large amounts of high-z star formation (Shull & Venkatesan 2008). Some of these simulations also include strong mechanical feedback from SN explosions. In particular, the dotted lines show a simulation with an early X-ray partial ionization and reheating. In this simulation metals are dispersed in the IGM mainly from the photoevaporation of low-mass galaxies. The solid and dashed lines show simulations with early reionization from Population III stars with top-heavy IMF and $\langle f_{esc} \rangle = 0.5$ (i.e., strong radiative feedback). The solid lines show a case where we also include strong feedback from SN explosions (e.g., Population III stars, having typical masses in the range $100 - 300$ M$_\odot$, some of which end their lives as pair-instability SNe). The dashed line shows a case in which energy input from SN explosions is negligible, such as Population III stars with masses < 140 M$_\odot$ or > 260 M$_\odot$, that end their lives collapsing into BHs without energetic SN explosions or without exploding at all.

The results show that low-mass galaxies are more effective than massive ones in enriching a large volume fraction of the IGM, but only to very low-metallicities. Supernova explosions, tidal stripping of metals, and photoevaporation of low-mass galaxies have similar importance for transporting metals from galaxies to the low density IGM.

We interpret the results shown in Figure 4 with the aid of a toy model, fitting the model to the simulation results. In order to calculate the volume of metal enriched gas, we integrate the contribution of each galaxy as a function of time to find the IGM porosity,

$$Q_V(Z > Z_0, t) = \frac{4\pi}{3} \int_0^t dt' \int_0^\infty \frac{dM_{\rm dm}}{M_{\rm dm}} \times \frac{\partial}{\partial t'} \left[n_{\rm gal}(M_{\rm dm}, t') R^3_{\rm met}(Z_0, M_{\rm dm}, t') \right] , \quad (1)$$

TABLE 2
Parameters: Volume Filling Factor of Metal-enriched Gas.

Name	RUN	A	α	$\langle Z/Z_\odot \rangle_M$	$\langle Z/Z_\odot \rangle_V$
S1	256L1p3	1.0	0.35	-2.84	-4.32
S2	128L1p2-2	1.9	0.35	-2.95	-4.19
S3	128L1p2f1	1.6	0.50	...	...
S4	128L1noRAD	3.4	0.30	-2.31	-3.56
S5	128L1XR	3.0	0.25	-3.71	-5.145
S6	128L2BH	5.0	0.35	-2.82	-4.056
S7	128L2PI	8.0	0.30	-2.28	-3.542

where $0 < Q_V < \infty$ is the porosity, $n_{\rm gal}(M_{\rm dm}, t)$ is the volume number density of galaxies of total mass $M_{\rm dm}$, and $R_{\rm met}(Z_0, M_{\rm dm}, t)$ is the radius of metal-enriched gas with metallicity $Z > Z_0$ around each galaxy. The volume filling factor is related to the porosity by the relationship $f_V \equiv 1 - \exp[-Q_V]$, so that $f_V \simeq Q$ if $Q \ll 1$, and $f_V = 1$ as $Q_V \to \infty$. Due to the effect of galaxy clustering this simple model may break down for relatively small values of f_V. The interpretation with our toy model of the results shown in the upper panels of Figure 4, for which $f_V > 1\%$, may be significantly inaccurate.

For fixed Z_0, we find that the porosity increases with time as $Q_V(t) \propto t^3$ within 20% error. Within the same error, the porosity of metal-enriched IGM with $Z > Z_0$ as a function of time is well approximated by the fitting formula,

$$Q_V(Z > Z_0) \simeq A \left(\frac{Z_0}{0.05 Z_\odot} \right)^{-\alpha} \left[\frac{t}{t_{z=9}} \right]^3 , \quad (2)$$

where $t_{z=9}$ is the Hubble time at $z = 9$ and the parameters A and α (Table 2) depend on the metal yield, the IMF, and the feedback processes included in the simulations.

The mean physical distance between small mass galaxies at high redshift is only a few kpc. In principle, these small galaxies may pollute the IGM quite uniformly with metals. However, the smaller the mass of the galaxy, the lower its ability to form stars and produce metals. For this reason, the metals ejected into the IGM by the more numerous population of small mass galaxies have a larger feeling factor than metals produced by more rare massive galaxies, but can only enrich the IGM to a very low metallicity floor.

We could assume, for simplicity, that galaxies of mass $M_{\rm dm} > M_0$ are responsible for the enrichment to a metallicity $Z > Z_0$. For galaxies of comoving spatial density $n_{\rm gal}$, the mean physical distance between star-forming galaxies is $d_{\rm gal} \approx n_{\rm gal}^{-1/3}/(1+z) \sim 1$–$30$ kpc, depending on their mass (see § 7). Given that the volume filling factor is between a few percent to 50% depending on Z_0, we estimate from equation (2) that $R_{\rm met} \sim 1$ kpc. Metal-enriched gas expanding at constant speed $v_{\rm ej}$ for a time t travels a distance,

$$R_{\rm met} = (1 \text{ kpc}) \left(\frac{v_{\rm ej}}{10 \text{ km s}^{-1}} \right) \left(\frac{t}{100 \text{ Myr}} \right) . \quad (3)$$

Since the Hubble time at high redshifts ($10 < z < 30$) is $t_H \sim 0.1 - 0.5$ Gyr and the bursting star formation has time scales $t_{\rm burst} \sim 10$ Myr, this distance requires that $10 < v_{\rm ej} < 100$ km s^{-1}. The lower bound of $v_{\rm ej}$ is about the escape velocity from dPri galaxies and is consistent

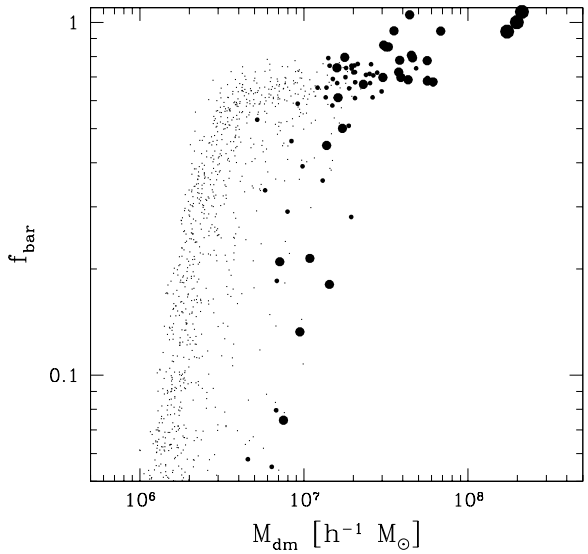

FIG. 5.— Fraction of baryons (sum of gas and stars) to dark matter (normalized to the cosmic mean value $f_{\rm bar}^{\rm max} = \Omega_b/\Omega_m = 0.136$) as function of the halo mass $M_{\rm dm}$ for run S1 at $z = 10$. The size of the dots is proportional to the fraction of stars $f_* = M_*/M_{\rm bar}^{\rm max}$ in each halo: from the largest to the smallest dots we have $f_* > 10\%$, $1 < f_* < 10\%$, $0.1 < f_* < 1\%$ and $f_* < 0.1\%$, respectively. The baryon content in dark halos (smallest dots) smaller than a few 10^6 $M_\odot$ drops sharply because of the finite IGM temperature (the mass cut of indeed is at smaller masses at earlier times when the IGM temperature is lower). In low-mass halos that form some stars, the baryon fraction is further decreased by photoheating from internal sources of radiation.

with metal pollution by processes (i) and (ii). Larger values of $v_{\rm ej}$ could be produced by SN explosions, but from equation (3) we infer that these higher velocities are in place for only a fraction of the Hubble time at $z \sim 10$.

We note that, if our simulation volume at $z \sim 8-9$ becomes a mean density or an underdense region of the universe at $z \sim 2-5$, the clustering and galaxy formation will be slow from $z \sim 8-9$ to $z \sim 2-5$, and the filling factor of metal-enriched gas should not increase considerably. The metallicity in overdense regions at $z \sim 2-5$ will be produced mostly by newly formed galaxies not included in our simulations.

6. POPULATION OF DWARF PRIMORDIAL GALAXIES

In this section we analyze the properties of the simulated population of dPri galaxies (their stellar and gas content as a function of total mass) and the internal properties of individual objects (gas and stellar density profiles).

6.1. *Statistical Properties of the Galaxies*

One of the most distinctive properties of simulated dPri galaxies is their low baryon-to-dark matter ratios. This is not too surprising, since in most of our simulations we include mechanical energy input from SN explosions. Most of the intergalactic gas that falls into the deep gravitational potential of massive galaxies and clusters is effectively trapped. In this case, it is a good approximation to assume that their total baryonic mass (the sum of gas and stars) is $M_{\rm bar}^{\rm max} \simeq (\Omega_b/\Omega_m)M_{\rm dm}$, where $\Omega_b/\Omega_m \simeq 1/6$ is the cosmic mean of the baryon-to-dark matter mass ratio. In Figure 5 we show the fraction of baryons in each simulated galaxy normalized to the cosmic mean, $f_b = (M_* + M_g)/M_{\rm bar}^{\rm max}$, as a function of their total mass $M_{\rm dm}$. The figure refers to run S1 at $z = 10$. The size of each circle represents the fraction of stars $f_* = M_*/M_{\rm bar}^{\rm max}$ in each galaxy. As expected, more massive galaxies retain on average a larger fraction of their initial baryon content, but the scatter of the $f_{\rm bar} - M_{\rm dm}$ relationship increases with decreasing halo mass. The baryon content in star-free halos (smallest dots) depends on the IGM temperature. When we examine the same plots as in Figure 5 but at redshifts $z \gtrsim 13$ we find $f_* \sim 1$. As the temperature of the IGM increases, the baryon fraction diminishes, first in the smaller halos and then in the larger ones. In those halos that form some stars, the baryon fraction is further reduced by photoevaporative winds produced by the internal sources of radiation. As a result, the distribution of the baryon fraction inside halos as a function of their mass depends on whether they are dark or luminous: the typical cut off mass decreases with decreasing f_* and eventually equals the minimum cut off mass set by the IGM temperature.

The large variations of the mass-to-light ratio and the gas fraction in halos of identical total mass is an indication of the local nature of the feedback processes. This is illustrated in Figure 6 that shows the stellar fraction $f_* = M_*/M_{\rm bar}^{\rm max}$ as a function of the halo mass, $M_{\rm dm}$, at $z = 10$ for the run S1 (left figure) and run S2 (right figure). Each galaxy is shown with symbols of different sizes proportional to their gas fraction. Halos of masses $M_{\rm dm} < 10^7$ $M_\odot$ can be completely dark (most of them), while low luminosity galaxies and a few brighter galaxies can have 10–50% of their gas converted into stars. The scatter is much reduced for galaxies with masses $M_{\rm dm} > 10^7$ $M_\odot$ that retain most of their gas, and their stellar fraction shows a much tighter relation to their total mass. At $z \sim 10$, galaxies with $M_{\rm dm} > 10^7$ $M_\odot$ are still gas rich, with a subdominant stellar component. The main physical processes responsible for the low efficiency of star formation are photoevaporation from internal sources and global feedback (e.g., photodissociation of H_2 and IGM reheating).

The mean values of the stellar and gas fractions as a function of the halo mass are shown in Figure 7. In the left panel, we show the mean as a function of DM mass at $z = 12.5, 9.6$, and 9 for run S1, and the right panel shows the same for run S2. Dwarf galaxies that form stars show large variations in their gas content because of stellar feedback and photoionization. The gas is photoevaporated first from low-mass galaxies and as time progress in larger ones. Luminous galaxies with $M_{\rm dm} < 10^8$ $M_\odot$ lose most their gas well before reionization and star formation is halted. New star formation cannot take place in those small halos unless their mass increases as a result of subsequent minor mergers.

We find that the mean star-formation efficiency $\langle f_*(t)\rangle = \langle M_*/M_{\rm bar,max}\rangle$ in a halo of mass $M_{\rm dm}$, is nearly time-independent and is well approximated by a power law

$$\langle f_*\rangle(t) \simeq \epsilon_* \left(\frac{M_{\rm dm}}{10^8\ {\rm M}_\odot}\right)^\alpha, \qquad (4)$$

where ϵ_* is the assumed star-formation efficiency. There

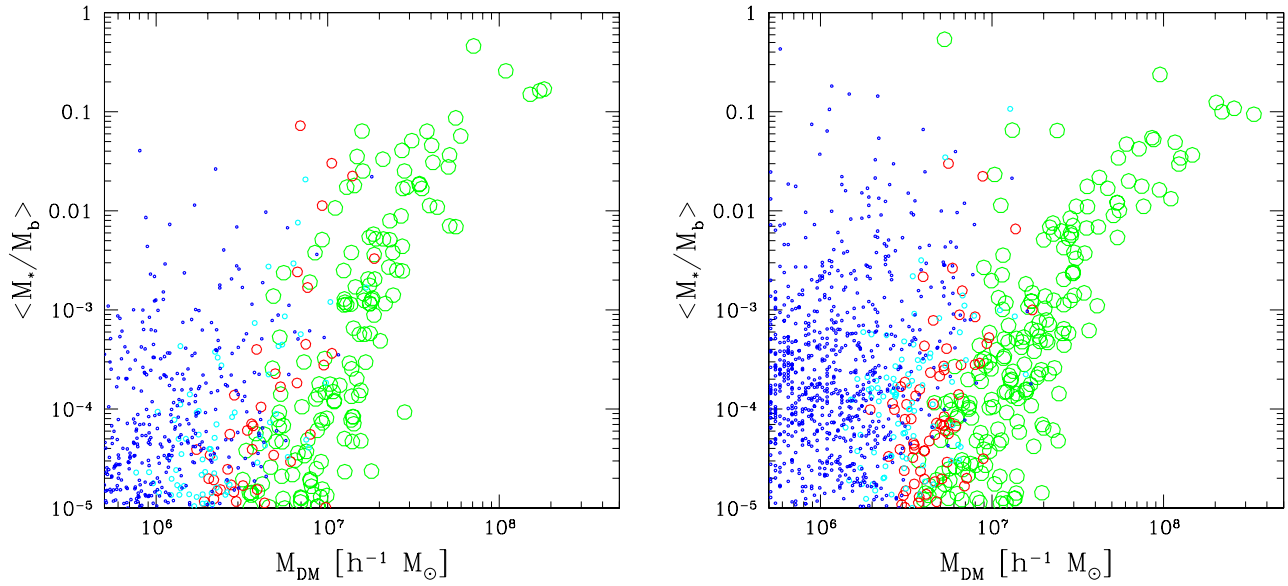

FIG. 6.— Fraction of gas converted into stars as function of halo mass of the galaxy for S1 run (left) and S2 (right) at $z = 10$. Circles, from smaller to the larger, refer to galaxies with gas fractions $f_g < 0.1\%$ (blue), $0.1\% < f_g < 1\%$ (cyan), $1\% < f_g < 10\%$ (red) and $f_g > 10\%$ (green), respectively. There is a clear lower envelope for the star formation efficiency, f_*, in halos with masses $> 10^7$ M$_\odot$, roughly proportional to the halo mass. The scatter of the values of f_* increases with decreasing halo mass and, remarkably, the upper envelope of $f_*(M_{\rm dm})$ is almost independent of the halo mass. This reflects the fact that local feedback plays an important role in determining the luminosity of low-mass galaxies.

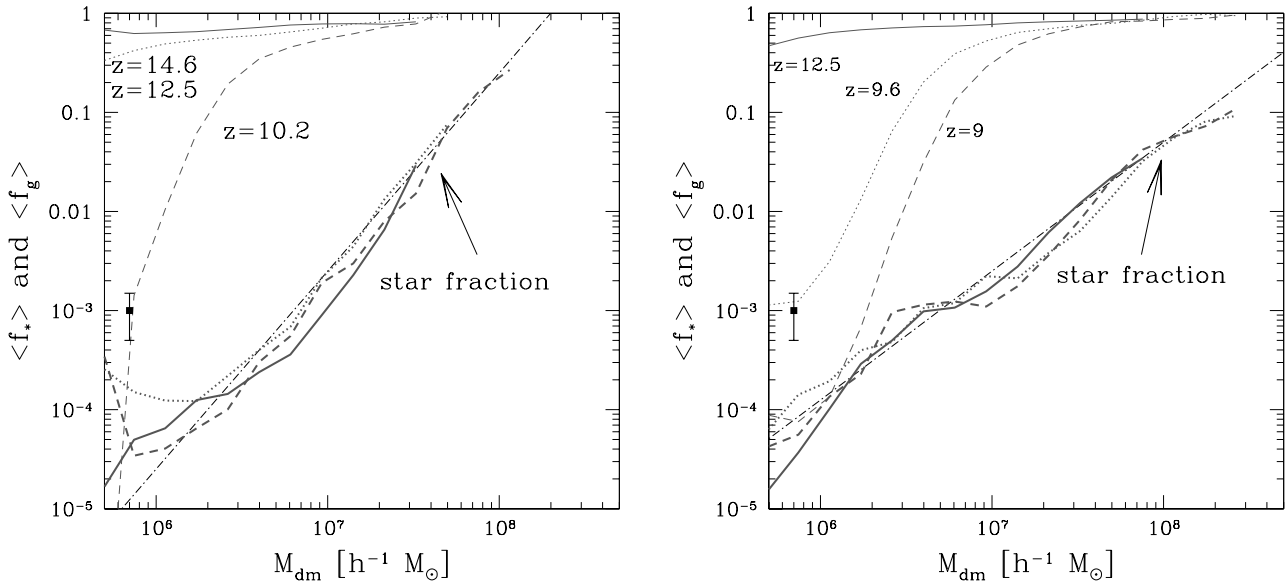

FIG. 7.— *(Left).* Average stellar fraction $\langle f_* \rangle$ (thick curves), and gas fraction $\langle f_g \rangle$ (thin curves), as a function of halo mass at $z = 14.6, 12.5$, and 10.2 for the run S1. *(Right).* Same as the left panel, for sun S2 at $z = 12.5, 9.6$, and 9. For comparison, the symbol with error bar shows the expected star formation efficiency in the first mini halo of mass 10^6 M$_\odot$ simulated by Abel et al. (2002).

is a weak dependence of the exponent in the power law on the strength of the feedback: $\alpha = 1.5$ if the feedback is weak (run S2) and $\alpha = 2$ if the feedback is stronger (run S1). However, contrary to what happens to the gas fraction, the stellar fraction does not evolve significantly with time. Equation (4) can be an useful approximation in semi-analytic models for galaxy formation. The point shown with a cross in Figure 7 is the first galaxy simulated with very high resolution by Abel et al. (2002). The point lies above the mean value for galaxies with mass $M = 10^7$ M$_\odot$. This is not surprising, because in our simulations most of the galaxies are dark, owing to feedback processes not included in simulations of the first stars.

6.2. *Metallicity Distribution of the Stars*

In this section we study the metallicity distribution of the first stars in the simulations from Paper 2. First,

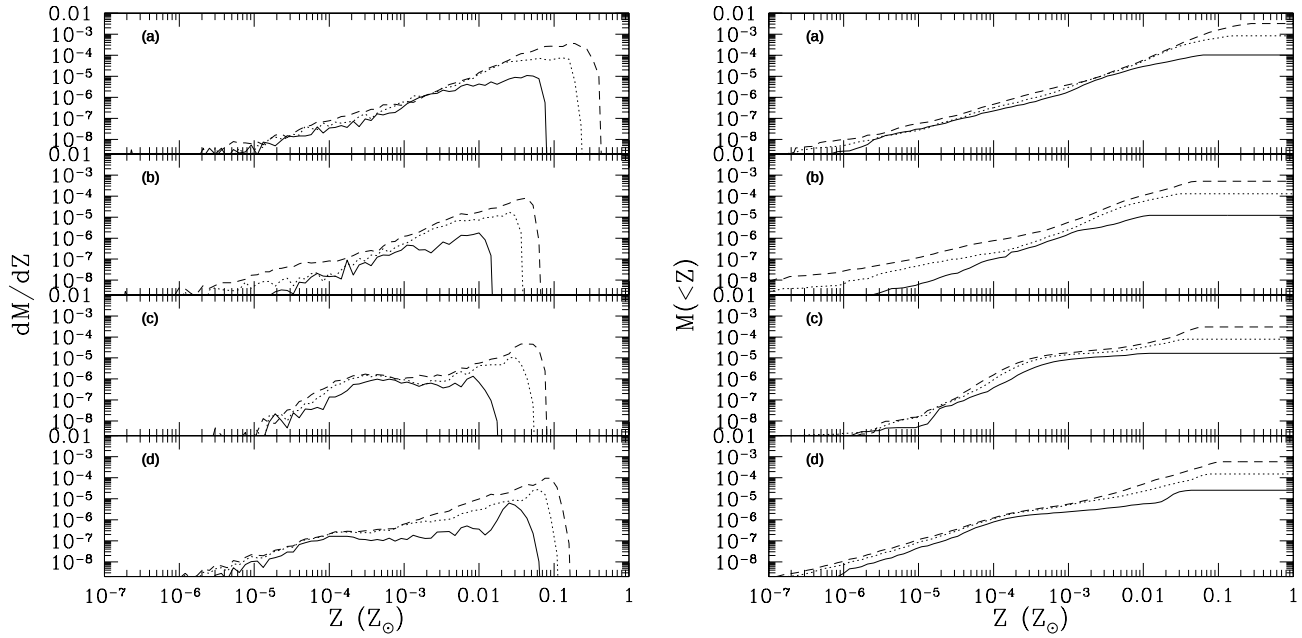

FIG. 8.— (*Left*). Mass fraction of stars as a function of their metallicity Z in solar units. Each panel refers to a different simulation, where solid, dotted and dashed lines show mass at $z = 17.5, 14.6$ and 12.5, respectively. In (a) we show run S4, in (b) run S2, in (c) run S3, and in (d) run S1. From top to bottom, feedback is stronger and the global mode of star formation changes from continuous to bursting. (*Right*). Same as left figure, but showing cumulative mass in stars with metallicity lower than Z.

we clarify the numerical limitations of the simulations, which do not attempt to model the mechanical energy input from SNe. The resolution of the simulation is insufficient to resolve the complexity of physical processes that regulate the physics of the multi-phase ISM. In each resolution element, we assume perfect metal mixing, although it is possible that the metal distribution is inhomogeneous on smaller scales. Thus, pockets of zero-metallicity gas may survive even if the gas has a large mean metallicity. As discussed in § 5, in those simulations where we have also included SN feedback, we find, in agreement with Gnedin (1998), that mechanical feedback does not affect star formation in galaxies with $M_{\rm dm} \gtrsim 10^8$ M$_\odot$. In lower mass galaxies, when we include the effect of SNe, the results are similar to simulations with strong photoevaporative galactic winds discussed in this section. Therefore, given the uncertainties introduced by the model-dependent treatment of SN explosions, we prefer to study only the cases that include the better understood radiative feedback.

Given the aforementioned caveat, Figure 8 (left) shows the mass fraction of stars as a function of their metallicity Z in solar units. Each panel refers to a different simulation, at $z = 17.5, 14.6$, and 12.5. In Figure 8 (right) we show the cumulative mass in stars with metallicity lower than Z expressed in solar units. In each panel, from top to bottom, we show the metallicity distribution in simulations with the following properties:
Panel (a): no feedback - star formation is continuous and there are no galactic winds due to SN explosions or photoionization. Some enriched gas might be lost from interacting galaxies by tidal stripping during galaxy interactions or mergers (Gnedin 1998). Metals can be accreted by larger galaxies when smaller satellites fall into them. In this simulation, the low-metallicity stars with $Z < 0.01$ Z$_\odot$ stop forming at redshift $z \sim 17$, and the mean metallicity of stars increases with time. By $z = 10$ most stars have $0.05 < Z/Z_\odot < 0.5$.
Panel (b): weak feedback - star formation is continuous and takes place also in very low-mass galaxies but with low efficiency. The formation of stars in these smaller galaxies is delayed, and zero-metallicity stars may continue to form at $z \sim 10$.
Panel (c): strong feedback - bursty star formation takes place only in higher mass galaxies and is suppressed in the smaller ones. There are fewer extremely low metallicity stars ($Z/Z_\odot < 10^{-5}$) and an uniform distribution between $Z/Z_\odot \sim 10^{-4}$ to 10^{-2}. After redshift $z \sim 10$, as low-metallicity stars stop forming, star formation takes place only in pre-enriched gas.
Panel (d): intermediate feedback and higher resolution - in this simulation the metallicity distribution of stars is an intermediate case between panel (b) and (c).

In order to estimate the number of low metallicity stars expected in the present day Universe from the data in our simulations, several assumptions need to be made. Here, we briefly describe how one should proceed in order to estimate the number of low-metallicity stars in our Galactic halo. Given our rather simplistic treatment, these numbers should be considered order of magnitude estimates. More sophisticated modeling could be adopted to compare the simulations to detailed observational data (Tumlinson 2006).

First, we note that even at redshifts $z \sim 10 - 20$ most stars have metallicities of about 1/10 solar, while only 1% have ultra low metallicities ($Z \lesssim 10^{-3}\ Z_\odot$). Let's assume that ultra low metallicity stars stop forming sometime before redshift $z \sim 10$: as it seems to be the case in all our simulations but S2, the one with weak radiative feedback. Using a rough estimate of the mass of stars that forms in the Universe after $z = 10$, we estimate a fraction of stars (in mass) in the present universe with metallicity $Z < 10^{-4}\ Z_\odot$ of roughly 10^{-6}.
The stars in our Galactic halo have total mass of about

10^{10} $M_\odot$. Therefore, assuming a uniform mixture of low and higher metallicity stars, a mass of about 10^4 $M_\odot$ of our Galactic halo should be in stars with $Z < 10^{-4}$ $Z_\odot$. Roughly, in our simulations, the number of low-metallicity stars decreases by a factor of ten, going down a decade in metallicity (see Figure 8). Thus, for stars with $Z < Z_{cr}$ where $Z_{cr} = 10^{-6}$, 10^{-5}, 10^{-4}, and 10^{-3} $Z_\odot$, the mass in the halos is $100, 1000, 10^4$, and 10^5 $M_\odot$, respectively. More precise estimates can be obtained using the metallicity distributions in Figure 8 for each simulation. Run S3, with strong feedback, gives smaller masses in ultra low-metallicity stars than run S2, that has weak feedback.

Finally, we need to know how many stars have masses $M_* \lesssim 1$ $M_\odot$, since more massive stars would evolve into unobservable compact remnants. Assuming a Salpeter IMF, we estimate that 100 $M_\odot$ in stars form about 100 stars with masses $M_* < 1$ $M_\odot$. Therefore, the aforementioned values for the mass in stars express also the number of ultra low metallicity stars, assuming a Salpeter IMF. If ultra low metallicity stars have a top-heavy IMF, their number in the halo will be smaller. If there is a critical metallicity that determines the transition from top-heavy to Salpeter IMF, this should produced an observable feature in the observed number counts of stars as a function of their metallicity, unless the transition from top-heavy to Salpeter IMF is smooth.

6.3. *Internal Properties of the Galaxies*

In this section we study the internal structure of selected galaxies in our highest resolution simulation (S1 in Table 1) that, in physical coordinates, has spatial resolution of about 10 pc at $z \sim 9-10$. The stellar component of simulated dPri galaxies is a low surface brightness spheroid that closely resembles dSph galaxies observed in the Local Group.

In Figure 9 we show the average density of gas (dots) and stars (squares) assuming spherical shells, as a function of the distance from the center of six galaxies selected from the simulation S1 at redshift $z \simeq 10$. The projected surface brightness, Σ (dashed lines), is shown on the right axis.

The gas density profile has a core of a few 100 pc in radius, comparable to the core radius of the stellar component. The mean gas density in the core is $n_H \approx 10-50$ cm^{-3}. The spatial resolution of the simulation is not sufficient to resolve fluctuations around this mean on scales smaller than 10-20 pc. It is therefore impossible to study the structure of the multi-phase ISM. But two interesting differences with respect to the Milky Way ISM structure can be noted. The mean gas density in the core is 10–50 times larger than the mean ISM density (~ 1 cm^{-3}) in the Milky Way. The gas and stellar component extend to the outer edges of the dark-matter halo. The virial radii of the dark halos are about 1000 pc, only a few times more extended. For comparison, the Milky Way stellar spheroid has radius of a few kpc and the virial radius is about 300 kpc. The mean temperature of the simulated ISM is $500 - 1000$ K, and the gas velocity dispersion is $\sigma_v \sim 10$ km s^{-1}, similar to the Milky-Way. The thermal pressure is therefore quite large, $P/k \sim 5 \times 10^3 - 5 \times 10^4$ cm^{-3} K, several times larger than in the Milky Way (Jenkins & Tripp 2001; Wolfire et al. 2003). The ISM mean metallicity is $Z \sim 0.1 - 0.01$ solar. Assuming that

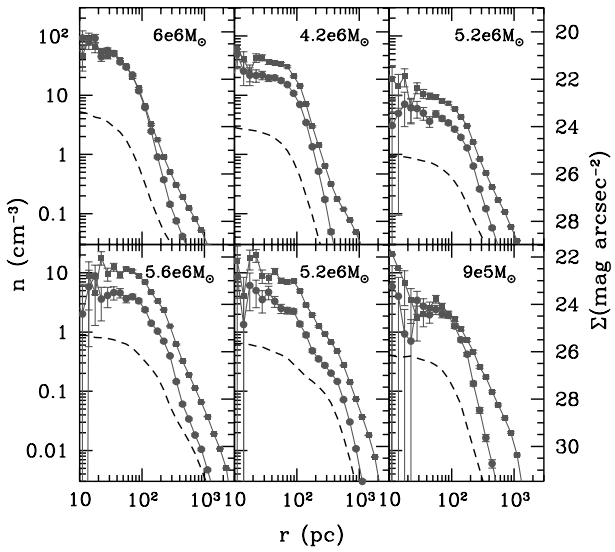

FIG. 9.— Azimuthally averaged gas (dots) and stellar (squares) projected density profiles of six galaxies selected from the simulation S1 at $z \sim 10$. For comparison, at virialization, the mean baryon density $\overline{n}_{vir} \sim 0.04$ cm^{-3}, and the density in the core is $n_{core} \sim 1$ cm^{-3}. The projected surface brightness, Σ (dashed lines), is shown on the right axis in units of magnitude per arcsec^2. The numbers shown on the top right corners in each panel refer to the totall mass in stars.

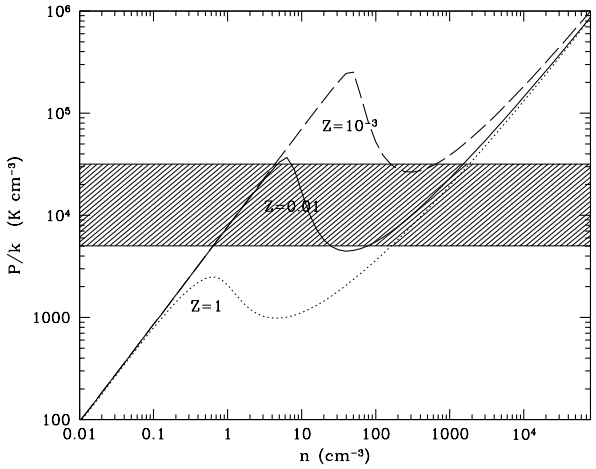

FIG. 10.— Phase diagram of the ISM at metallicities $Z/Z_\odot$ = 1, 0.01, and 10^{-3}. The ISM in our simulated dPri galaxies have metallicities $Z = 0.01 - 0.1$ $Z_\odot$ and thermal pressures in the range shown by the cross-hatched band. Therefore, the conditions are compatible with a multi-phase ISM, where dense clouds and intercloud gas can coexist in a gas roughly at pressure equilibrium (at least in a broad statistical sense).

the ISM is in pressure equilibrium and including all relevant cooling and heating processes as in Wolfire et al. (1995), we have calculated the phase diagram (thermal pressure as a function of density) for a gas of metallicity Z (see Ricotti et al. 1997, for details of the calculation). The dotted, solid and dashed lines in Figure 10 show the

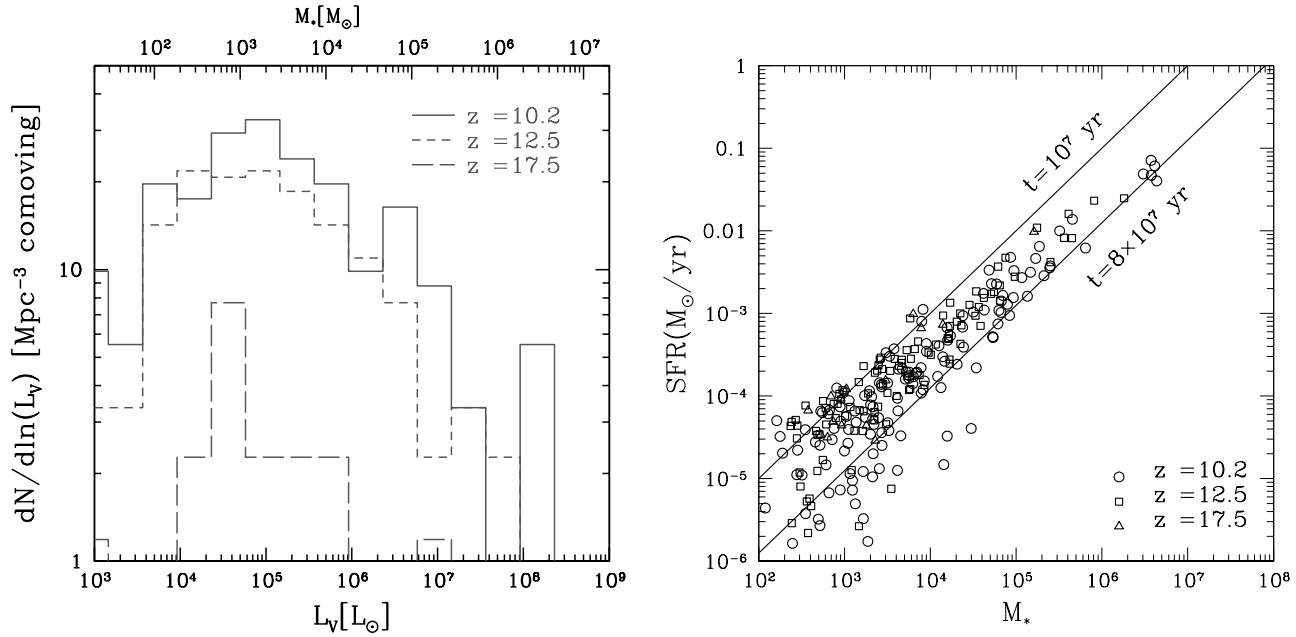

FIG. 11.— (*Left*). Number density of primordial galaxies at redshifts $z = 10.2, 12.5$, and 17.5 as a function of their luminosity (or stellar mass) for the simulation S1. (*Right*). Star formation rate as a function of stellar mass for galaxies at redshifts $z = 10.2, 12.5$, and 17.5 in the simulation S1. The two lines that bracket most of the points show the star formation rate as a function of M_* assuming that all the stars formed in a single burst of duration $t_{\rm burst} = 10$ and 80 Myr.

phase diagram of the ISM with metallicity $Z/Z_\odot = 1$, 0.01, and 10^{-3}, respectively. For constant pressure, if the gas has metallicity $Z = 0.01$ $Z_\odot$ and the pressure is in the range shown by the shaded band, there are three possible equilibrium values for the density: the low-density value is thermally stable and is called warm neutral medium (WNM), the intermediate density value is thermally unstable, and the high-density value is stable and called cold neutral medium (CNM). If the pressure lies outside this interval, a multi-phase medium in which dense clouds (CNM) and inter-cloud gas (WNM) coexist cannot develop. From the values of the pressure and metallicity in our simulated dPri galaxies, we expect that a multi-phase ISM should be sustained.

We now return to the properties of the stellar component. Most simulated dark matter halos form stars very inefficiently or do not form stars at all. The gas density profiles in these dark galaxies are similar to the ones shown in Figure 9 and have a mean molecular hydrogen abundance $x_{H_2} \sim 10^{-4}$. The high density of the gas in these dark galaxies may have important implications for reionization, through increases in the clumping of the IGM. In luminous galaxies the stellar component is a spheroid with negligible angular momentum compared to the stellar velocity dispersion. The spheroid has low surface brightness, but it is relatively extended, with outer edges reaching $\sim$ 20% of the virial radius, substantially more extended than in present-day galaxies. The most luminous galaxies in the simulation have surface brightness between 23-27 mag arcsec^{-2}, comparable to that of dSph galaxies in the Local Group and Andromeda (e.g., 26.8 AndIX, 25.5 Ursa Minor, 25.3 Draco, 24.5 And III). Detailed comparisons with the properties of dSph galaxies was the subject of a separate paper (Ricotti & Gnedin 2005). The properties of the the dark matter halos were also discussed in separate papers (Ricotti 2003; Ricotti & Wilkinson 2004) since they seem to show cores instead of cusps, in agreement with many observations of dwarf spheroidal galaxies and LSB galaxies (e.g., Kleyna et al. 2003; Magorrian 2003; de Blok et al. 2003).

7. OBSERVABILITY OF DWARF PRIMORDIAL GALAXIES

In this section, we study the feasibility of observing dPri galaxies during their formation at redshifts $9 < z < 30$. In particular, we calculate the number of point sources in the infrared bands detectable in the field of view of the JWST. Then, we briefly address the prospects for the identification of the fossil records of dPri galaxies in the Local Group. Even if most dPri galaxies merge into larger systems after their formation, a fraction of them (approximatively 10%) is expected to survive to $z = 0$. These relics could be observed today as satellites of larger galaxies or in isolation. We compare the mass function of the satellites observed around the Milky Way and Andromeda with the simulated mass function of luminous halos. For realistic values of the survival probablity, our simulations, which include radiative feedback but not the effect of reionization, can reproduce the observed mass function of Galactic satellites.

7.1. *Detection of Primordial Galaxies with JWST*

The luminosity function of dPri galaxies at redshifts $z = 10.2, 12.5$, and 17.5 is shown in the Figure 11 (left) for simulation S1. We assumed a mass-to-light ratio $M_*/L_V = 1/50$ (solar), appropriate for starbursts with age $t \sim 100$ Myr. The panel on the right shows the star formation rate as a function of the stellar mass for the same galaxies. The two lines show the values of the mean star formation rate (SFR) that would produce a stellar mass, M_*, in a single burst of durations $t_{\rm burst} = M_*/SFR \simeq 10$ Myr and 80 Myr.

About 10% of dwarf sized dark matter halos with $M_{\rm dm} > 10^6$ $M_\odot$ that assembled prior to reionization

are able to form stars. There are $\sim$ 500 dPri galaxies per Mpc^3 with luminosities spanning four decades, between 10^4 and 10^8 L$_\odot$. The luminosity function is rather flat, with $\sim$ 10 galaxies Mpc^{-3} in the higher luminosity decade ($10^7 < L < 10^8$ L$_\odot$) and 200 Mpc^{-3} in the fainter decade ($10^4 < L < 10^5$ L$_\odot$).

The integrated number counts of galaxies at $z > 9$ in the IR bands is shown in Figure 12. The solid lines show the number counts at $z <$ and $z <$ derived from the simulation data. The dashed lines are extrapolations of the bright end of the luminosity function to account for more massive galaxies not present in our simulations due to their small volume. The dashed lines are calculated using Press-Schechter formalism to derive the number counts of dark halos and assuming a stellar mass in each of them that is a constant fraction of their total mass (hence neglecting feedback). The assumed constant value of the star formation efficiency is the same as for the most massive halos present in the simulation. Although the counts are uncertain, especially at the bright end of the luminosity function, Figure 12 clearly shows that JWST will not be able to detect any of the small mass galaxies formed in our simulations.

For a Salpeter IMF and $\langle f_{esc} \rangle \sim 1$, JWST might be able to detect the most massive galaxies at redshift $z \sim 10$. But the prospects for observing the formation of the fainter low-mass galaxies that cool by H_2 is very small. The number of faint sources will not be able to resolve the controversy of whether dark halos with $M < 10^8$ M$_\odot$ host luminous galaxies, or have their formation suppressed by H_2-dissociating radiation. But it may be possible to infer the slope of the luminosity function below the sensitivity limit of the JWST by analyzing the fluctuation of the unresolved background (see for example, Miyaji & Griffiths 2002, for a technique applied to the *Chandra* deep field). Only if the IMF in dPri galaxies is top-heavy and $\langle f_{esc} \rangle \ll 1$ the luminosity of dPri galaxies in the K bands (rest frame UV) at the same mass will be up to 10 times higher than in Figure 12. In this second case, it may be possible to use the faint number counts to constrain the theoretical models and quantify the relative importance of negative and positive feedback on the formation of dPri galaxies.

7.2. *Relics of Primordial Dwarf Galaxies*

How many galaxies that formed the bulk of their stars before reionization, do we expect to observe in the Local Universe? In CDM cosmologies, galaxies similar to the Milky Way were formed by accreting the debris of old, lower-mass galaxies and the intergalactic gas surrounding them. However, most low-mass galaxies that were the dominant galaxy population at high redshift, have been destroyed and incorporated into larger galaxies, constituting a fraction of their bulge and halo stars. The probability that a galaxy formed at redshift z_f survives without being incorporated into a larger one is roughly $(1 + z_f)^{-1}$ (e.g., Sasaki 1994). Therefore, about 10% of the galaxies in our simulations are expected to survive to the present. Since the total number of low-mass galaxies per h^{-3} Mpc^3 at $z = 10$ is 10–100, the number of fossil primordial galaxies today should be about $1 - 10$ per Mpc^3 h^{-3}.

A detailed study on the identification of the fossils of the first galaxies in the Local Group is the focus of two previous works (Ricotti & Gnedin 2005; Gnedin & Kravtsov 2006). In (Ricotti & Gnedin 2005, , hereafter RG05), we have focused on comparing observable properties of the population of primordial dwarf galaxies from our high-resolution simulation (run S1), to the properties of Local Group dwarf galaxies. In RG05 we have evolved the run S1 to lower redshift and have introduced a strong source of ionization in the simulated volume that fully reionize the IGM (see the paper for details). After reionization, due to the increase of the IGM Jeans mass, low-mass halos are devoided of all gas and are not able to form new stars because gas accretion is suppressed by IGM reheating. Hence, the subset of galaxies in our simulation that survives tidal stripping, can be compared to present day galaxies simply by aging passively their stellar populations. The striking similarities between the properties simulated galaxies and many Local Group dSphs lead us to propose a scenario for their origin as the surviving well-preserved fossils of the first galaxies. In addition, the simulation shows the existence of a population of ultra-faint dwarf galaxies, not observed at the time of publication. This ultra-faint population may have been recently discovered in the Local Group (Belokurov et al. 2007, 2006; Irwin et al. 2007; Willman et al. 2005b,a; Walsh et al. 2007; Zucker et al. 2006b,a; Ibata et al. 2007; Majewski et al. 2007; Martin et al. 2006).

Gnedin & Kravtsov (2006), presented a detailed study of the prediction of the simulation in RG05, on the probability of survival of the fossils of dPri galaxies as they are incorporated in a Milky Way type halo. The results of this study show that the galactocentric distribution of the simulated galaxies reproduce the observed distribution of normal dwarf around the Milky-Way, but the ultra-faint population of simulated dwarfs was not accounted for at the time of publication. Finally, in Bovill & Ricotti (2008) we show that the prop-

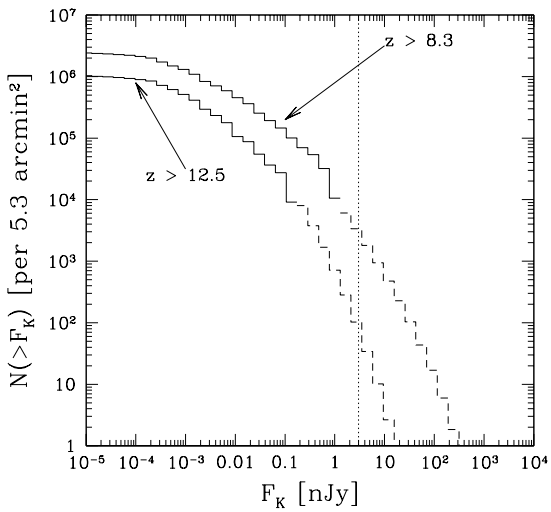

FIG. 12.— Cumulative number counts of primordial galaxies in the K bands at redshifts $z \gtrsim 9$ in our higher resolution simulation (S1). Similar results are obtained for the other simulations. Assuming a Salpeter (top-heavy) IMF, dwarf primordial galaxies with masses $M_{\rm dm} > 10^8$ M$_\odot$ ($M_{\rm dm} > 10^7$ M$_\odot$) are luminous enough to be detectable with the JWST, if it operates at nominal sensitivity shown by the vertical line (NIRCAM has a sensitivity of 3 nJy in the F200W and F277W filters for 10^5 sec exposures).

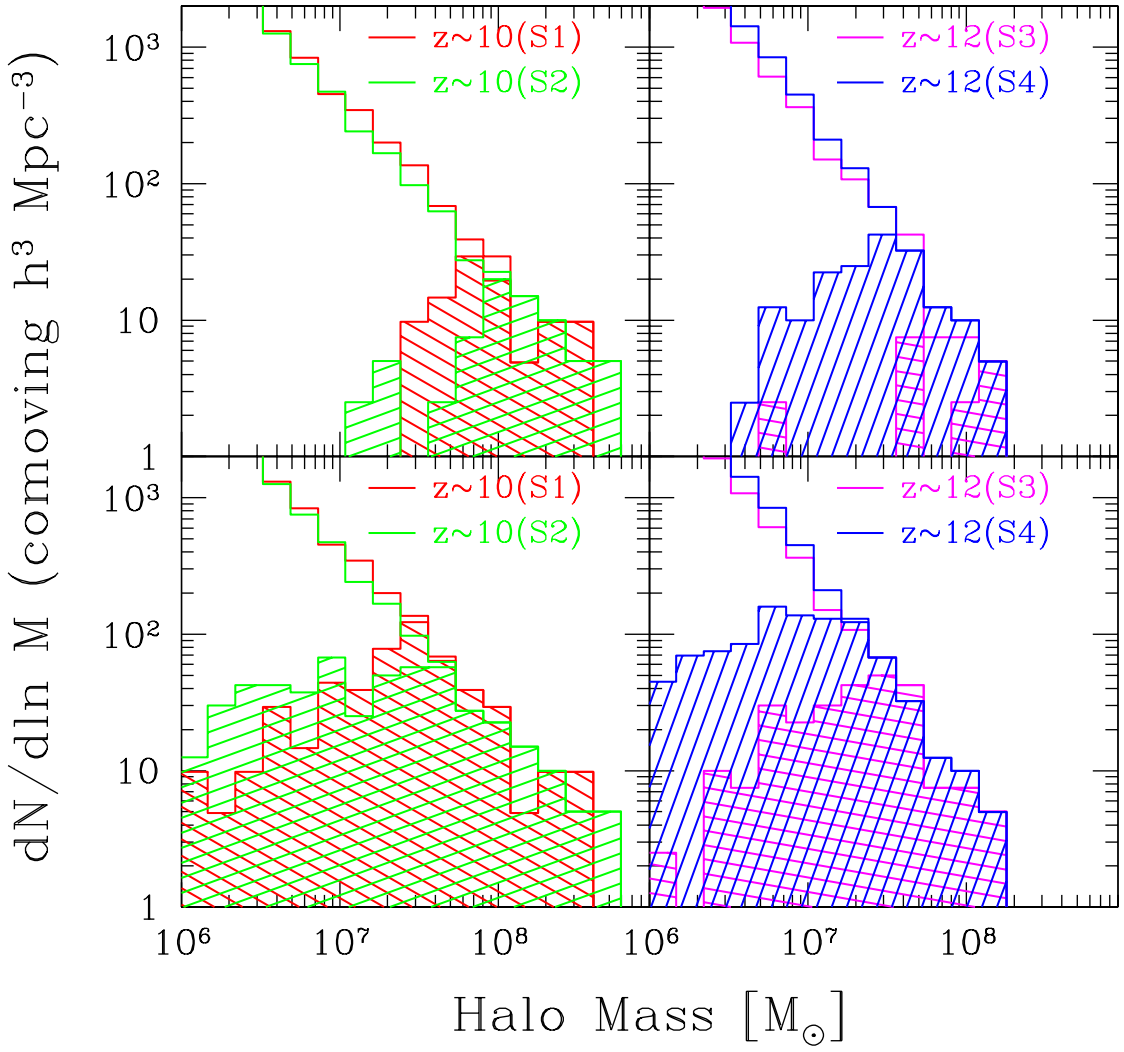

FIG. 13.— Mass function of dark matter halos (histograms) and luminous galaxies (shaded histograms) at $z \approx 10$ in four simulations from Table 1. The left panels show run S1 (high-resolution run) and run S2. The right panels show run S3 (strong radiative feedback) and S4 (without radiative feedback). The shaded histograms in the two top panels display the mass function of dwarf galaxies with $M_* \geq 5 \times 10^5$ $M_\odot$ (or $L_V \gtrsim 10^5$ $L_\odot$ assuming an old stellar population) and the bottom panels with $M_* \geq 5 \times 10^3$ $M_\odot$ (or $L_V \gtrsim 10^3$ $L_\odot$), thus including ultra-faint dwarfs.

erties of the newly discovered population of dwarf galaxies matches the theoretical prediction in RG05 and (Gnedin & Kravtsov 2006). The galactocentric distribution of the recently discovered population of ultra-faint dwarfs nearly closes the gap between observations and theoretical predictions, hence solving the well know "missing galactic satellite problem".

In this section we focus on another well know observed property of the normal population (as opposed to the ultra-faint one, with $L_V < 10^5$ $L_\odot$ or $M_V \lesssim -7.7$) of dwarf galaxies in the Local Group: there seems to be a characteristic dynamical mass of about 10^7 $M_\odot$. One may be tempted to assume that this mass is the smallest galactic halo mass, or the galaxy building block. However, some of the newly discovered ultra-faint dwarfs have dynamical masses that are smaller than in the normal population (Simon & Geha 2007). Here, comparing different simulations in Table 1, we show that radiative feedback processes determine the value of the characteristic mass of 10^7 $M_\odot$ in the normal population of dSphs, and that the strength of radiative feedback determines the number and characteristic mass (typically $< 10^7$ $M_\odot$), of the ultra-faint dwarf population. In order to fully understand the origin and the physics of the mass cut-off, much more work is needed. This study goes beyond the scope of the present paper and will be explored separately.

The shaded histograms in Figure 13 show the mass function of galaxies at $z \approx 10$ (i.e., luminous halos) compared to the mass function of all halos (i.e., dark and luminous) in four simulations from Table 1. The shaded histograms in the top panels show the mass function of "normal" dwarf galaxies with $L_V \geq 10^5$ $L_\odot$ ($M_V < -7.7$), while the two bottom panels include also ultra-faint dwarfs with $L_V \geq 10^3$ $L_\odot$. Run S1 (the high resolution run) and run S2 (the run with weak radiative feedback) are shown in the left panels. Run S3 with

strong feedback, and run S4 withouth radiative feedback are shown in the righ panels. The panels illustrate two important properties of the first galaxies:
1) Dwarfs that have luminosities comparable or larger than Ursa Minor or Draco (top panels), have a mass function with a characteristic mass cut off $M_{dm} \sim 10^7$ $M_\odot$, in agreement with observations (e.g., Mateo 1998). The mass cut off is not a numerical artifact - it is lower in the lower resolution runs S2 and S3 than in the higher resolution run, S1. Clearly, the mass cutoff is produced by radiative feedback, as it is not present in the simulation without radiative feedback, S4, and it is weakly dependent on the strength of feedback (e.g., compare run S2 and S3).
2) The simulations show the existence of a population of ultra-faint dwarfs with $L_V < 10^5$ $L_\odot$ (bottom panels). The mass function of this ultra-faint population extends down to the smallest masses resolved in our simulations, or shows a smaller lower mass cut off than in normal dwarfs. If feedback is strong as in run S2, the ultra faint galaxies are fewer and have larger typical masses than in the runs with weak or no radiative feedback.

Here, it is important to recall our definition of strong and weak feedback: whether a simulations has weak or strong radiative feedback, depends on the intensity of ultraviolet radiation that escapes into the IGM. Hence, a run with top-heavy IMF and $\langle f_{esc} \rangle \sim 1$ is a simulation with strong feedback, while a run with Salpeter IMF and $\langle f_{esc} \rangle < 1$ corresponds to a simulation with weak feedback.

8. SUMMARY AND CONCLUSIONS

In this paper, the third of a series, we have analyzed in detail the properties of the first galaxies in a set of three-dimensional cosmological simulations. This paper is devoted to the analysis of statistical and internal properties of the population of dPri galaxies and their impact on the IGM.

In the first part (Paper 1) of this study, we addressed the problem of simulating the formation of the first galaxies by implementing a cosmological code that includes time-dependent, three-dimensional radiative transfer of H I , He I and He II ionizing photons in a cosmological volume. Using a recipe for star formation and a fast method to solve radiative transfer (Gnedin & Abel 2001) at each hydro time-step, we were able to simulate the radiative feedback processes by the first luminous sources. We modelled the physics of chemically pristine gas including a non-equilibrium treatment of the chemistry of nine species (e^-, H, H^+, He, He^+, He^{+2}, H_2, H_2^+, H^-), cooling by molecular hydrogen, ionization by secondary electrons, Lyα pumping, and radiative transfer for the narrow lines in the H_2 Lyman-Werner bands of the dissociating background radiation. Currently, these simulations are the state of the art for the formation of dPri galaxies, in the sense that are the only simulations that include time-dependent and spatially inhomogeneous radiative feedback processes without introducing sub-grid analytical recipes.

In the second part of this study (Paper 2) we found that, contrary to previous work, dPri galaxies are able to form enough stars to be cosmologically important. The reasons for disagreement of our results with previous ones may be due to the density-dependent reformation rate of H_2 (quickly photodissociated in the voids, but not in the denser filaments) and time-dependent feedback produced by the bursting mode of star formation (e.g., H_2 reformation in relic H II regions) or a combination of both. These processes are not included in previous semi-analytic studies and numerical simulations (Machacek et al. 2001; Tassis et al. 2003). Our simulations do not include the effect of H_2 self-shielding by photodissociating radiation, so it is possible that we are underestimating star formation in lower-mass galaxies. However, we have shown that the global star formation rate is self-regulated and insensitive to the intensity of the photodissociating background. In most simulations (see Table 1) we did not include mechanical feedback by SN explosions, motivated by previous results (Gnedin 1998) showing that their effect is negligible unless we adopt a top-heavy IMF. The effect of SN explosions depends strongly on the particular implementation in the code and is difficult to test. The method for solving radiative transfer has instead been tested on simple benchmark problems, but a better test of the reliability of our results will need to wait for other simulations that include a similar self-consistent treatment of radiative transfer and feedback.

In the following list we summarize the main conclusions of our simulations of properties of our sample of dPri galaxies and their effects on the metallicity of the IGM.

1. *Number and luminosity of dPri galaxies.* About 10% of dwarf dark matter halos ($M_{\rm dm} > 10^6$ $M_\odot$) assembled prior to reionization are able to form stars. We find ~ 500 dPri galaxies per $\rm Mpc^3$ between 10^4 and 10^8 $L_\odot$. The luminosity function is rather flat, with 10 galaxies $\rm Mpc^{-3}$ ($10^7 < L < 10^8$ $L_\odot$) and 200 $\rm Mpc^{-3}$ at ($10^4 < L < 10^5$ $L_\odot$).

2. *Relative importance of H_2 and metal cooling.* H_2 cooling is important for the formation of the first few stars in each protogalaxy. As the first few stars form, if the ISM has not been blown out, Lyα and metal-line cooling become dominant. If radiative feedback is strong (top-heavy IMF) star formation in lower mass dark halos is suppressed. If the feedback is weak (Salpeter IMF and/or small $\langle f_{esc} \rangle$), star formation in lower-mass galaxies is inefficient and delayed, but not suppressed.

3. *Clustering.* The local nature of feedback has implications for the clustering and bias properties of the first luminous galaxies. Analogous to young star clusters at low-redshift, these form preferentially in groups and chain-like structures and are more clustered than the dark halos of the same mass.

4. *Volume filling factor of metal-enriched IGM.* The metals produced by the first galaxies can fill the space between bright galaxies rather uniformly, but only to very low values of the metallicity ($Z/Z_\odot \lesssim 10^{-5}$). The volume filling factor of the IGM enriched to the typical metallicities observed in the Lyα forest is small. It is unlikely that the metal absorption systems seen in the Lyα forest were produced by the first low-mass galaxies.

5. *Gas photoevaporation.* Star-forming dwarf galaxies show large variations in their gas content because

of the combined effects of stellar feedback from internal sources and IGM reheating. Ratios of gas to dark matter lie below the cosmic mean in halos with masses $M_{\rm dm} < 10^8$ M$_\odot$. Gas depletion increases with decreasing redshift: the lower-mass halos lose all their gas first but, as the universe evolves, larger halos with $M_{\rm dm} \sim 10^8$ M$_\odot$ also lose a large fraction of their gas.

6. *Mean star-formation efficiency.* The mean star formation efficiency $\langle f_*(t) \rangle = \langle M_*/M_{\rm bar}^{\rm max} \rangle$. We assume that $M_{\rm bar}^{\rm max} \simeq M_{\rm dm}/7$, with an efficiency independent of redshift and depending on total mass as $\langle f_*(t) \rangle \propto M_{\rm dm}^{\alpha}$. There is weak dependence on feedback: $\alpha = 1.5$ if the feedback is weak and $\alpha = 2$ if the feedback is strong.

7. *Scatter of the mass-to-light ratio.* A tight relationship between the star formation efficiency f_* and the total mass of halos holds only for galaxies with $M_{\rm dm} > 5 \times 10^7$ M$_\odot$. In lower-mass halos, the scatter around the mean $\langle f_* \rangle$ is increasingly large. For a given halo mass, the galaxy can be without stars (dark galaxy, $f_* = 0$) or have $f_* \sim 0.5$. A few dark galaxies as massive as $M_{\rm dm} \sim 1 - 5 \times 10^7$ M$_\odot$ may exist in the Local Group.

8. *Low-metallicity stars.* The mass fraction of Population III stars (metallicity $Z < 10^{-3}$) with respect to Population II stars is about one in a million at $z = 10$. The epoch dominated by Population III stars is short-lived. In models with strong feedback, it ends at $z \sim 17$, while if the feedback is weak, a small fraction of Population III stars is still forming at $z = 10$. About $N = 1000(Z_0/10^{-3}Z_\odot)$ stars with metallicity smaller than a floor Z_0 should be present in the Galactic halo for a Salpeter IMF. If the feedback is strong, the distribution of low-metallicity stars has a sharp drop at $Z \simeq 10^{-4}$ Z$_\odot$ and is almost flat at $10^{-4} < Z/Z_\odot < 10^{-2}$. Furthermore, if there is a transition from a Salpeter IMF to top-heavy IMF at a critical value of the stellar metallicity ($Z < Z_{\rm cr}$), the distribution should show a cutoff at that critical metallicity.

9. *Luminosity profile.* Galaxies with masses $M < 10^8$ M$_\odot$ have a low surface brightness and extended stellar spheroid. The outer edges of the stellar spheroid nearly reaches the virial radius. In more massive galaxies that cool efficiently by Lyα radiation, the stars and light are more centrally concentrated.

10. *Multi-phase interstellar medium.* The interstellar medium (ISM) of these galaxies has mean density $10 - 100$ cm^{-3} and thermal pressure $P/k \sim 10^5$ cm^{-3} K. This pressure is sufficiently high to develop a multi-phase ISM in low metallicity gas ($10^{-2} - 10^{-3}$ $Z_\odot$).

11. *Deep field number counts.* For a Salpeter IMF, JWST might detect only the most massive dPri galaxies. The prospects for observing the formation of the fainter low-mass galaxies that cool by H_2 is very small. If, instead, the IMF in dPri galaxies is top-heavy and $\langle f_{esc} \rangle \ll 1$, JWST might be able to detect dPri galaxies with masses as small as $M_{\rm dm} \sim 10^7$ M$_\odot$. In this second case, the faint number counts could constrain theoretical models and quantify the relative importance of negative and positive feedback for their formation.

12. *Typical masses of dSphs and ultra-faint dwarfs in the Local Group.* Radiative feedback suppresses star formation in low-mass halos. Halos with $M_{dm} > 10^7$ M$_\odot$ produce galaxies with luminosities typical of normal dSphs such as Ursa Minor and Draco. Halos with $M_{dm} < 10^7$ M$_\odot$ may host a population of ultra-faint dwarfs, similar to the one recently discovered in the Local Group, or may be completely dark.

This work was supported by the Theoretical Astrophysics program at the University of Colorado (NASA grant NNX07AG77G and NSF grant AST07-07474) and at the University of Maryland (NASA grant NNX07AH10G). The simulations were performed using SGI/CRAY Origin 2000 array at the National Center for Supercomputing Applications (NCSA).

REFERENCES

Abel, T., Bryan, G. L., & Norman, M. L. 2002, Science, 295, 93
Adelberger, K. L., Steidel, C. C., Shapley, A. E., & Pettini, M. 2003, ApJ, 584, 45
Ahn, K., & Shapiro, P. R. 2007, MNRAS, 375, 881
Belokurov, V., et al. 2007, ApJ, 654, 897
Belokurov, V., et al. 2006, ApJ, 647, L111
Bovill, M., & Ricotti, M. 2008, in preparation
Bovill, M., Ricotti, M., Gnedin, Y., & Kravstov, A. 2008, in preparation
Bromm, V., Coppi, P. S., & Larson, R. B. 1999, ApJ, 527, L5
Couchman, H. M. P., & Rees, M. J. 1986, MNRAS, 221, 53
de Blok, W. J. G., Bosma, A., & McGaugh, S. 2003, MNRAS, 340, 657
Ferrara, A. 1998, ApJ, 499, L17
Ferrara, A., Pettini, M., & Shchekinov, Y. 2000, MNRAS, 319, 539
Fujita, A., Mac Low, M.-M., Ferrara, A., & Meiksin, A. 2004, ApJ, 613, 159
Gnedin, N. Y. 1998, MNRAS, 294, 407
Gnedin, N. Y., & Abel, T. 2001, New Astronomy, 6, 437
Gnedin, N. Y., & Kravtsov, A. V. 2006, ApJ, 645, 1054
Haiman, Z., Abel, T., & Rees, M. J. 2000, ApJ, 534, 11
Haiman, Z., & Bryan, G. L. 2006, ApJ, 650, 7
Haiman, Z., Rees, M. J., & Loeb, A. 1996, ApJ, 467, 522
Ibata, R., Martin, N. F., Irwin, M., Chapman, S., Ferguson, A. M. N., Lewis, G. F., & McConnachie, A. W. 2007, ApJ, 671, 1591
Irwin, M. J., et al. 2007, ApJ, 656, L13
Jenkins, E. B., & Tripp, T. M. 2001, ApJS, 137, 297
Johnson, J. L., & Bromm, V. 2007, MNRAS, 374, 1557
Kleyna, J. T., Wilkinson, M. I., Gilmore, G., & Evans, N. W. 2003, ApJ, 588, L21
Lavery, R. J., & Mighell, K. J. 1992, AJ, 103, 81
Machacek, M. E., Bryan, G. L., & Abel, T. 2001, ApJ, 548, 509
Machacek, M. E., Bryan, G. L., & Abel, T. 2003, MNRAS, 338, 273
Madau, P., Ferrara, A., & Rees, M. J. 2001, ApJ, 555, 92
Madau, P., Meiksin, A., & Rees, M. J. 1997, ApJ, 475, 429
Madau, P., Rees, M. J., Volonteri, M., Haardt, F., & Oh, S. P. 2004, ApJ, 604, 484
Magorrian, J. 2003, in The Mass of Galaxies at Low and High Redshift. Proceedings of the ESO Workshop held in Venice, Italy, 24-26 October 2001, p. 18.
Majewski, S. R., et al. 2007, ApJ, 670, L9
Martin, N. F., Ibata, R. A., Irwin, M. J., Chapman, S., Lewis, G. F., Ferguson, A. M. N., Tanvir, N., & McConnachie, A. W. 2006, MNRAS, 371, 1983
Mateo, M. L. 1998, ARA&A, 36, 435
Miller, J. M., Fabbiano, G., Miller, M. C., & Fabian, A. C. 2003, ApJ, 585, L37
Miyaji, T., & Griffiths, R. E. 2002, ApJ, 564, L5
Moore, B., Ghigna, S., Governato, F., Lake, G., Quinn, T., Stadel, J., & Tozzi, P. 1999, ApJ, 524, L19
Oh, S. P. 2001, ApJ, 553, 499
Oh, S. P., & Haiman, Z. 2002, ApJ, 569, 558
Pasquali, A., Larsen, S., Ferreras, I., Gnedin, O. Y., Malhotra, S., Rhoads, J. E., Pirzkal, N., & Walsh, J. R. 2005, AJ, 129, 148
Pettini, M., Madau, P., Bolte, M., Prochaska, J. X., Ellison, S. L., & Fan, X. 2003, ApJ, 594, 695
Ricotti, M. 2003, MNRAS, 344, 1237
Ricotti, M., Ferrara, A., & Miniati, F. 1997, ApJ, 485, 254
Ricotti, M., & Gnedin, N. Y. 2005, ApJ, 629, 259
Ricotti, M., Gnedin, N. Y., & Shull, J. M. 2001, ApJ, 560, 580
Ricotti, M., Gnedin, N. Y., & Shull, J. M. 2002a, ApJ, 575, 33
Ricotti, M., Gnedin, N. Y., & Shull, J. M. 2002b, ApJ, 575, 49
Ricotti, M., & Ostriker, J. P. 2004a, MNRAS, 350, 539
Ricotti, M., & Ostriker, J. P. 2004b, MNRAS, 352, 547
Ricotti, M., Ostriker, J. P., & Gnedin, N. Y. 2005, MNRAS, 357, 207
Ricotti, M., & Wilkinson, M. I. 2004, MNRAS, 353, 867
Santoro, F., & Shull, J. M. 2006, ApJ, 643, 26
Sasaki, S. 1994, PASJ, 46, 427
Schaye, J., Aguirre, A., Kim, T., Theuns, T., Rauch, M., & Sargent, W. L. W. 2003, ApJ, 596, 768
Shull, J. M., & Venkatesan, A. 2008, ApJ, in press
Simcoe, R. A., Sargent, W. L. W., & Rauch, M. 2004, ApJ, 606, 92
Simon, J. D., & Geha, M. 2007, ApJ, 670, 313
Songaila, A. 2001, ApJ, 561, L153
Spergel, D. N., et al. 2007, ApJS, 170, 377
Susa, H., & Umemura, M. 2004, ApJ, 600, 1
Tassis, K., Abel, T., Bryan, G. L., & Norman, M. L. 2003, ApJ, 587, 13
Tegmark, M., Silk, J., Rees, M. J., Blanchard, A., Abel, T., & Palla, F. 1997, ApJ, 474, 1
Tumlinson, J. 2006, ApJ, 641, 1
Venkatesan, A., Giroux, M. L., & Shull, J. M. 2001, ApJ, 563, 1
Venkatesan, A., & Truran, J. W. 2003, ApJ, 594, L1
Walsh, S. M., Jerjen, H., & Willman, B. 2007, ApJ, 662, L83
Whalen, D., & Norman, M. L. 2008, ApJ, 673, 664
Whiting, A. B., Hau, G. K. T., & Irwin, M. 1999, AJ, 118, 2767
Willman, B., et al. 2005a, AJ, 129, 2692
Willman, B., et al. 2005b, ApJ, 626, L85
Wolfire, M. G., Hollenbach, D., McKee, C. F., Tielens, A. G. G. M., & Bakes, E. L. O. 1995, ApJ, 443, 152
Wolfire, M. G., McKee, C. F., Hollenbach, D., & Tielens, A. G. G. M. 2003, ApJ, 587, 278
Yoshida, N., Abel, T., Hernquist, L., & Sugiyama, N. 2003, ApJ, 592, 645
Zucker, D. B., et al. 2006a, ApJ, 650, L41
Zucker, D. B., et al. 2006b, ApJ, 643, L103